


# MUL1-RING recruits the substrate, p53-TAD as a complex with UBE2D2-UB conjugate

Min-Sung Lee<sup>1,2</sup>, Sang-Ok Lee<sup>1,3</sup>, Joonhyeok Choi<sup>4</sup>, Minju Ryu<sup>1,2</sup>, Mi-Kyung Lee<sup>1,2</sup>, Ji-Hun Kim<sup>3</sup>, Eunha Hwang<sup>4</sup>, Chong-Kil Lee<sup>3</sup>, Seung-Wook Chi<sup>1,2</sup> and Kyoung-Seok Ryu<sup>4,5</sup> 

1 Disease Target Structure Research Center, Division of Biomedical Research, KRIBB, Daejeon, South Korea

2 Department of Proteome Structural Biology, KRIBB School of Bioscience, University of Science and Technology, Daejeon, South Korea

3 College of Pharmacy, Chungbuk National University, Cheongju-si, South Korea

4 Ochang Center, Korea Basic Science Institute, Cheongju-Si, South Korea

5 Department of Bio-Analytical Science, University of Science and Technology, Daejeon, South Korea

## Keywords

MUL1 RING domain; NMR; p53 transactivation domain; UBE2D2; ubiquitin

## Correspondence

S.-W. Chi, Disease Target Structure Research Center, Division of Biomedical Research, KRIBB, Daejeon 34141, South Korea

Tel: +82-42-860-4277

E-mail: swchi@kribb.re.kr

K.-S. Ryu, Ochang Center, Korea Basic Science Institute, 162 Yeongudanji-Ro, Ochang-Eup, Cheongju-Si, Chungcheongbuk-Do 28119, South Korea

Tel: +82-43-240-5064

E-mail: ksryu@kbsi.re.kr

Min-Sung Lee, Sang-Ok Lee and Joonhyeok Choi contributed equally to this work.

(Received 20 June 2021, revised 6 January 2022, accepted 18 January 2022)

doi:10.1111/febs.16360

The RING domain of MUL1 (RING<sub>MUL1</sub>) alone mediates ubiquitylation of the p53-transactivation domain (TAD<sub>p53</sub>). To elucidate the mechanism underlying the simultaneous recruitment of UBE2D2 and the substrate TAD<sub>p53</sub> by RING<sub>MUL1</sub>, we determined the complex structure of RING<sub>MUL1</sub>:UBE2D2 and studied the interaction between RING<sub>MUL1</sub> and TAD<sub>p53</sub> in the presence of UBE2D2-UB thioester (UBE2D2~UB) mimetics. The RING<sub>MUL1</sub>-binding induced the closed conformation of UBE2D2<sup>S22R/C85S</sup>-UB<sup>K48R</sup> oxyester (UBE2D2<sup>RS</sup>-UB<sup>ROE</sup>), and strongly accelerated its hydrolysis, which was suppressed by the additional N77A-mutation of UBE2D2. Interestingly, UBE2D2<sup>S22R/N77A/C85S</sup>-UB<sup>K48R</sup> oxyester (UBE2D2<sup>RAS</sup>-UB<sup>ROE</sup>) already formed a closed conformation in the absence of RING<sub>MUL1</sub>. Although TAD<sub>p53</sub> exhibited weak binding for RING<sub>MUL1</sub> or UBE2D2 alone, its binding affinity was enhanced and even further for RING<sub>MUL1</sub>:UBE2D2 and RING<sub>MUL1</sub>:UBE2D2<sup>RAS</sup>-UB<sup>ROE</sup>, respectively. The recognition of TAD<sub>p53</sub> by RING<sub>MUL1</sub> as a complex with UBE2D2~UB is related to the multivalency of the binding events and underlies the ability of RING<sub>MUL1</sub> to ubiquitylate the intrinsically disordered protein, TAD<sub>p53</sub>.

## Introduction

Mitochondrial E3 ubiquitin ligase 1 (MUL1), located in the mitochondrial outer membrane, regulates various biological processes, including mitochondrial dynamics, cell growth, apoptosis, and mitophagy through ubiquitylation and SUMOylation [1]. It is a potential therapeutic target for Parkinson's disease

because its role is similar to that of the PINK1/Parkin pathway [2,3]. MUL1 also has different names, such as mitochondrial-anchored protein ligase (MAPL) [4], mitochondrial ubiquitin (UB) ligase activator of NF-κB (MULAN) [5], growth inhibition, and death E3 ligase (GIDE) [6] and Hades [7]. Sequence-based

## Abbreviations

CS, chemical shift; CSP, chemical shift perturbation; IDP, intrinsically disordered protein; ITC, isothermal titration calorimetry; RDC, residual dipolar coupling; RING<sub>MUL1</sub>, RING domain of MUL1; SEC, size exclusion chromatography; TAD<sub>p53</sub>, p53-transactivation domain; UB, ubiquitin; UBE2D2~UB, UBE2D2-UB thioester; UBE2D2-UB<sub>IP</sub>, UBE2D2-UB isopeptide; UBE2D2-UB<sub>OE</sub>, UBE2D2-UB oxyester.

topology analysis indicated that the major portion of MUL1, which lies between two transmembrane  $\alpha$ -helices (residues 9–29 and 239–259), is located in the mitochondrial intermembrane region, while the C-terminal RING domain (RING<sub>MUL1</sub>) faces the cytoplasm [6]. RING<sub>MUL1</sub> activity is critical for the ubiquitylation of mitofusin, Akt, p53, and ULK1, and responsible for the SUMOylation of dynamin-related protein 1 (Drp1) [1]. MUL1 plays a role in apoptosis via the direct regulation of apoptosis-associated proteins such as NF- $\kappa$ B, Akt, and p53, for which the activity of RING<sub>MUL1</sub> is critical [6–9].

Mitochondrial E3 ubiquitin ligase 1 negatively regulates the exonuclear function of p53 in the mitochondria via ubiquitylation. Moreover, results from cell-based *in vivo* and *in vitro* studies, including pull-down and immunoprecipitation experiments, showed that RING<sub>MUL1</sub> alone results in the ubiquitylation of p53 [7]. Although the six Lys residues in the C-terminal region of p53 are ubiquitylated by Mdm2 [10], the K24 residue of p53 is specifically ubiquitylated by the action of RING<sub>MUL1</sub> alone [7]. It has also been reported that RING<sub>MUL1</sub> ubiquitylates the transactivation domain (TAD<sub>p53</sub>, residues 1–73) in the presence of three E2 enzymes (UBE2D1, D2, and D3), but not by UBE2L3 (UbcH7) [11].

Ubiquitylation is generally mediated by the action of the following three enzymes: UB-activating E1, conjugating E2, and ligase E3. E3 plays a key role in determining the target specificity and catalysing UB-transfer from E2 to the Lys side-chain of the target protein, and is mainly classified into two groups according to their E2-binding domains (HECT and RING/U-box); Transfer of the attached donor UB (UB<sub>D</sub>) directly from E2 to the substrate protein is the key feature of ubiquitylation by RING-E3 [12]. RING-E3 ligase generally contains another domain or region that can facilitate the recruitment of a target protein [13]. Thus, the mechanism underlying the ubiquitylation of p53 by the action of RING<sub>MUL1</sub> alone seems to be unique. Although our recent NMR studies have indicated that non-labelled RING<sub>MUL1</sub> clearly binds <sup>15</sup>N-labelled TAD<sub>p53</sub> (<sup>15</sup>N-TAD<sub>p53</sub>), its binding affinity ( $K_d$ , 1.03 mM) is too weak to support the *in vivo* ubiquitylation activity of RING<sub>MUL1</sub> alone [14].

To elucidate the mechanism by which RING<sub>MUL1</sub> alone results in the recruitment and ubiquitylation of TAD<sub>p53</sub>, we determined the crystal structure of the RING<sub>MUL1</sub>:UBE2D2 complex, and then studied the detailed interactions between TAD<sub>p53</sub> and the RING<sub>MUL1</sub> complexes with UBE2D2 and UBE2D2~UB mimetics in solution. Additionally, we reported the distinguishing features of RING<sub>MUL1</sub> that

markedly enhanced the hydrolysis rate of UBE2D2~UB oxyester (UBE2D2~UB<sub>OE</sub>), and different dynamic natures of UBE2D2~UB<sub>OE</sub> depending on the N77 residue of UBE2D2. The higher binding affinity of TAD<sub>p53</sub> for RING<sub>MUL1</sub>:UBE2D2~UB<sub>OE</sub> than that for RING<sub>MUL1</sub> or UBE2D2 alone depended on the multivalency of their binding, which resulted from the innate characteristics of the intrinsically disordered protein (IDP), TAD<sub>p53</sub>.

## Results

### UBE2D2 exhibits a weak binding affinity for TAD<sub>p53</sub>

We first estimated the binding affinity between <sup>15</sup>N-TAD<sub>p53</sub> and UBE2D2 via chemical shift perturbation (CSP) experiments using two-dimensional (2D) <sup>1</sup>H–<sup>15</sup>N heteronuclear single quantum correlation (HSQC), since the ubiquitylation reaction is also mediated by the action of E2. Certainly, UBE2D2 also bound to <sup>15</sup>N-TAD<sub>p53</sub> ( $K_d$ , 735 ± 39  $\mu$ M; Fig. 1A and Table 1), in which the region containing residues A39 to D55 (AD39) displayed a higher CSP than that exhibited by the region containing residues, S15 to N29 (SN15). The marked decrease in the peak intensities of <sup>15</sup>N-TAD<sub>p53</sub> caused by the binding of RING<sub>MUL1</sub> with a higher  $K_d$  value, compared to that caused by the same concentration of UBE2D2, was likely from the heterogeneity of chemical shifts (CSs) induced by the structural flexibility of RING<sub>MUL1</sub> (Fig. 1A,B).

Reciprocal CSP experiments of <sup>15</sup>N-UBE2D2 in the presence of TAD<sub>p53</sub> and AD39 showed that their binding surfaces of UBE2D2 were almost identical, and mainly localized at two regions (Fig. 1E,F) as follows: (a) the main location was in the vicinity of the RING-binding site ( $\alpha$ 1 and N-terminal  $\alpha$ 3), while (b) the other location was on the rear side of UBE2D2 ( $\beta$ 4-to-loop and  $\alpha$ 4; Fig. 1J). The fact that the CSP amount of <sup>15</sup>N-UBE2D2 induced by the TAD<sub>p53</sub>-binding was considerably higher than that induced by the same concentration of AD39 indicated that the SN15 region also contributed to the binding of UBE2D2. We also ascertained the CSP amounts of <sup>15</sup>N-RING<sub>MUL1</sub> induced by TAD<sub>p53</sub> [14], and compared them to those corresponding to similar concentrations of AD39 and SN15. The CSP patterns of <sup>15</sup>N-RING<sub>MUL1</sub> demonstrated by TAD<sub>p53</sub>, AD39, and SN15 were similar, but the CSP amount was higher for TAD<sub>p53</sub> (Fig. 1G–I). Since each RING<sub>MUL1</sub> and UBE2D2 displayed a weak affinity to TAD<sub>p53</sub>, it was possible that the larger complexes (RING<sub>MUL1</sub>:UBE2D2 or RING<sub>MUL1</sub>:UBE2D2~UB) display a higher affinity for TAD<sub>p53</sub>.

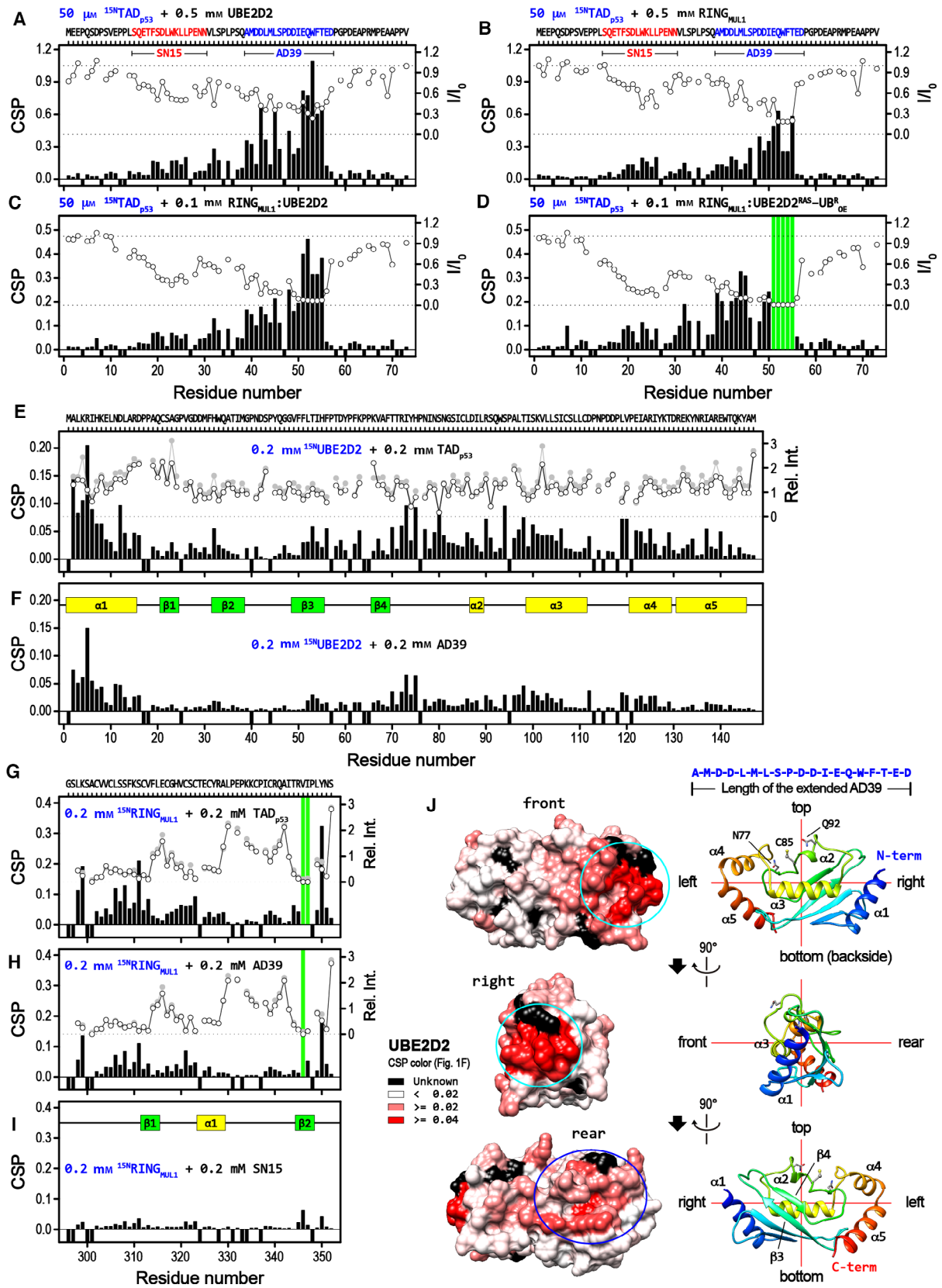


**Fig. 1.** The interactions of TAD<sub>p53</sub>, UBE2D2, and RING<sub>MUL1</sub> for different counterparts were studied by <sup>1</sup>H-<sup>15</sup>N HSQC experiments. The CSPs of <sup>15</sup>N-TAD<sub>p53</sub> (A–D), <sup>15</sup>N-UBE2D2 (E, F), and <sup>15</sup>N-RING<sub>MUL1</sub> (G–I) in the presence of interacting counterparts are shown as bar plots. The residues for which the HSQC crosspeaks were not shown in the free form and the peaks disappeared during the CSP experiments are shown as negative and green bars, respectively. (J) The AD39-binding surfaces of <sup>15</sup>N-UBE2D2 (panel-F) are shown following the degree of CSPs: (a) the front and right side, residues 2–16 (α1) and 94–103 (N-terminal α3), (b) the rear side, residues 70–75 (β4-to-loop) and 119–126 (α4). The reference orientation was defined for UBE2D2 (top, bottom, right and left, front and rear, respectively). The length of AD39 in an extended conformation is comparable to that of the long axis of UBE2D2.

**Table 1.** Binding constants ( $K_d$ , μM) measured by NMR CSP<sup>a</sup> and ITC ( $n$ , Δ*H*, kcal·mol<sup>-1</sup>) experiments.

	$K_d$ (μM)	$n$	Δ <i>H</i> (cal·mol <sup>-1</sup> )	Δ <i>S</i> (cal·mol <sup>-1</sup> ·deg <sup>-1</sup> )
<sup>15</sup> N-TAD <sub>p53</sub> + UBE2D2 <sup>a</sup>	735 ± 39	–	–	–
<sup>15</sup> N-TAD <sub>p53</sub> + RING <sub>MUL1</sub> :UBE2D2 <sup>a</sup>	171 ± 38	–	–	–
UBE2D2 + RING <sub>MUL1</sub>	<b>28 ± 15<sup>b</sup></b>	<b>0.71 ± 0.08<sup>b</sup></b>	<b>1479 ± 906<sup>b</sup></b>	<b>26.0 ± 4.3<sup>b</sup></b>
	13 ± 3	0.65 ± 0.13	2518 ± 571	30.9
	43 ± 18	0.80 ± 0.18	858 ± 247	22.8
	28 ± 10	0.69 ± 0.20	1061 ± 381	24.4
RING <sub>MUL1</sub> :UBE2D2 + AD39	<b>184 ± 13<sup>b</sup></b>	<b>0.88 ± 0.01<sup>b</sup></b>	<b>–1134 ± 16<sup>b</sup></b>	<b>13.3 ± 0.1<sup>b</sup></b>
	175 ± 34	0.89 ± 0.25	–1145 ± 372	13.4
	193 ± 29	0.87 ± 0.08	–1123 ± 130	13.2
RING <sub>MUL1</sub> :UBE2D2 + TAD <sub>p53</sub>	111 ± 31	1.01 ± 0.21	–673 ± 177	15.8
RING <sub>MUL1</sub> :UBE2D2 <sup>RAS</sup> -UB <sup>ROE</sup> + AD39	<b>129 ± 22<sup>b</sup></b>	<b>1.29 ± 0.32<sup>b</sup></b>	<b>–629 ± 125<sup>b</sup></b>	<b>15.7 ± 0.7<sup>b</sup></b>
	105 ± 20	1.65 ± 0.16	–598 ± 76	16.2
	151 ± 21	1.11 ± 0.16	–719 ± 122	15.1
	116 ± 16	0.95 ± 0.12	–466 ± 71	16.4
	143 ± 23	1.47 ± 0.16	–735 ± 102	15.1
RING <sub>MUL1</sub> :UBE2D2 <sup>RAS</sup> -UB <sup>ROE</sup> + TAD <sub>p53</sub>	<b>34 ± 16<sup>b</sup></b>	<b>0.67 ± 0.19<sup>b</sup></b>	<b>485 ± 71<sup>b</sup></b>	<b>20.6 ± 4.3<sup>b</sup></b>
	22 ± 4	0.54 ± 0.03	380 ± 31	22.6
	26 ± 6	0.58 ± 0.05	538 ± 63	22.8
	57 ± 24	0.95 ± 0.33	516 ± 211	21.2
	33 ± 7	0.62 ± 0.05	505 ± 59	22.2

<sup>a</sup>The HSQC peaks of the AD39 region of TAD<sub>p53</sub> were traced to obtain the  $K_d$  values.; <sup>b</sup>The average value and standard deviation of the multiple measurements.; The bold values are the average values of the multiple measurements.

### Crystal structure of RING<sub>MUL1</sub> in the RING<sub>MUL1</sub>:UBE2D2 complex

The crystal structure of the RING<sub>MUL1</sub>:UBE2D2 complex was solved at 2.7 Å resolution (Fig. 2A) by molecular replacement (MR) using the previous UBE2D2 coordinate. The structure of RING<sub>MUL1</sub> alone was solved at 1.8 Å resolution by the MR using the RING<sub>MUL1</sub> coordinate in the determined complex structure (Table S1). The crystal of UBE2D2 alone was also obtained during the crystal screens of the RING<sub>MUL1</sub>:UBE2D2 complex (Table S1), and the structure (1.8 Å resolution) was almost identical with the previously reported structures (PDB, 2CLW, and 2ESK). Although we also attempted to co-crystallize the RING<sub>MUL1</sub> complexes along with UBE2D2<sup>S22R/C85K</sup>-UB<sup>K48R</sup> isopeptide (UBE2D2<sup>RK</sup>-UB<sup>RIP</sup>), and UBE2D2<sup>S22R/N77A/C85S</sup>-UB<sup>K48R</sup> oxyester (UBE2D2<sup>RAS</sup>-UB<sup>ROE</sup>), and RING<sub>MUL1</sub>:UBE2D2<sup>RAS</sup>-UB<sup>ROE</sup> complex with the 2,4-dinitrophenyl dye-linked AD39 peptide, in which the

colour of the dye was used to determine the specific complex crystal containing the AD39 peptide, the results were unsuccessful.

The failure of molecular replacement (MR) with the NMR ensemble structures of RING<sub>MUL1</sub> (PDB, 6k2k) could be attributed to the structural discrepancy in the region containing residues 329–334 (Fig. 2B). Since the crystal structures of RING<sub>MUL1</sub> are consistent with the <sup>15</sup>N-<sup>1</sup>H residual dipolar coupling (RDC) data of <sup>15</sup>N-RING<sub>MUL1</sub> measured in solution (Fig. 2C), the discrepancy might arise from missing NOE-assignments during the previous automatic CYANA calculation. The greater deviation of the calculated RDC values among the six conformers of the higher resolution crystal structures of the RING<sub>MUL1</sub> alone reflected the existence of innate structural heterogeneity in solution, which substantiated the heterogeneous peak intensity of its HSQC spectrum [14]. The RDC values calculated for the four conformers of RING<sub>MUL1</sub> in the

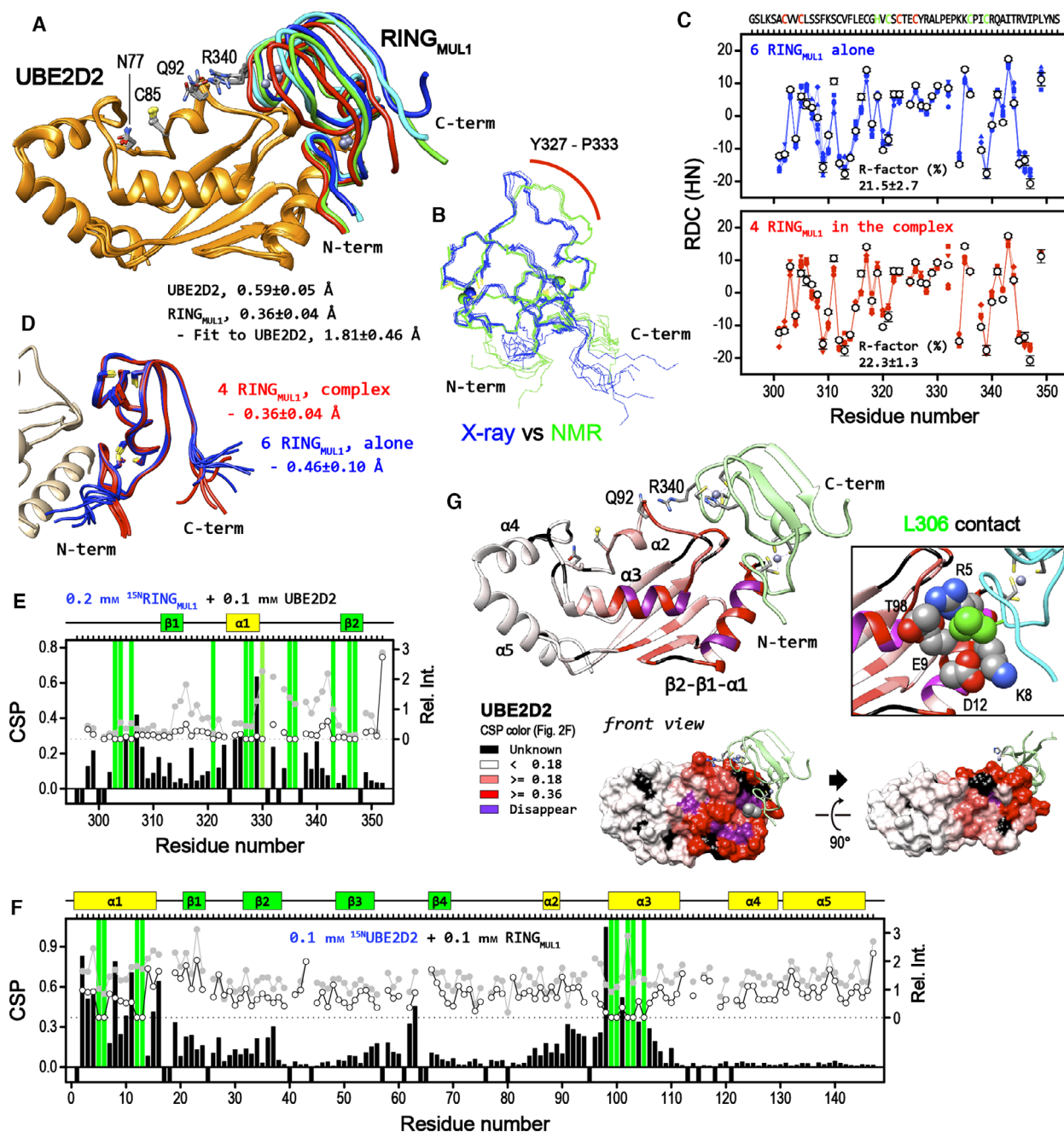


**Fig. 2.** Characterizations of the RING<sub>MUL1</sub>:UBE2D2 interaction by X-ray and NMR. (A) Four conformers in the crystal structure of RING<sub>MUL1</sub>:UBE2D2 are superimposed on the basis of UBE2D2. The pairwise RMSD values were calculated for the backbone atoms (CA, C, O, and N) of the well-structured regions (UBE2D2, M1–Y145; RING<sub>MUL1</sub>, A301–P348). The RMSD value of the RING<sub>MUL1</sub> part greatly increases from 0.36 to 1.81 Å, when their coordinates of four conformers were fixed to the superimposed UBE2D2. (B) The previous NMR ensemble structures (PDB, 6K2K; green) were overlaid with the six superimposed conformers of the RING<sub>MUL1</sub> crystal structure. (C) The <sup>1</sup>H–<sup>15</sup>N RDC values of <sup>15</sup>NRING<sub>MUL1</sub> measured in solution (open circle) were compared to the crystal structures of RING<sub>MUL1</sub> alone (blue) and RING<sub>MUL1</sub> in the complex with UBE2D2 (red). (D) The six conformers of the RING<sub>MUL1</sub> structure (blue) alone are superimposed with the four RING<sub>MUL1</sub> molecules of the RING<sub>MUL1</sub>:UBE2D2 complex (red). The CSPs of <sup>15</sup>NRING<sub>MUL1</sub> (E) and <sup>15</sup>NUBE2D2 (F) in the presence of non-labelled UBE2D2 and RING<sub>MUL1</sub>, respectively are shown as bar plots with the same colours used before. (G) The CSPs of <sup>15</sup>NUBE2D2 induced by RING<sub>MUL1</sub> (panel-F) are mapped to the UBE2D2 structure. RING<sub>MUL1</sub> binding considerably perturbed the specific regions of UBE2D2 ( $\alpha$ 1-to- $\beta$ 2, and  $\alpha$ 3 segments) that are used for the binding of UB<sub>BS</sub> and the UB<sub>D</sub>. The residues of UBE2D2 that are close to L306 of RING<sub>MUL1</sub> (< 3.5 Å) are shown as a sphere model (boxed).

complex were less variable, indicating that its structure was ordered by the UBE2D2-binding (Fig. 2C).

There are six and four molecules present in the asymmetric units of the RING<sub>MUL1</sub> and RING<sub>MUL1</sub>:UBE2D2 crystals, respectively. Structural comparison between RING<sub>MUL1</sub> alone and complexes showed no appreciable change had occurred in RING<sub>MUL1</sub>, except in the N- and C-terminal regions of RING<sub>MUL1</sub> (Fig. 2D). R340 of RING<sub>MUL1</sub> belongs to the previously characterized F-x(K/R) motif (F, a hydrophobic amino acid; x, the Cys of the Zn<sup>+2</sup>-finger; I338-C339-R340 in RING<sub>MUL1</sub>) of the RING<sub>E3</sub> domain that acts as a linchpin to enable the activation of E2~UB [15], and the side-chain of R340 that is in close contact with Q92 of UBE2D2 in the RING<sub>MUL1</sub>:UBE2D2 complex (Fig. 2A). Interestingly, the overlay of the four conformers of the RING<sub>MUL1</sub>:UBE2D2 complex showed that the positional plasticity of RING<sub>MUL1</sub> molecules was relative to UBE2D2 (Fig. 2A). The backbone root-mean-square deviation (RMSD) values of RING<sub>MUL1</sub> and UBE2D2 among the four conformers in the complex structures are  $0.59 \pm 0.05$  and  $0.36 \pm 0.04$  Å, respectively. The RMSD value of four RING<sub>MUL1</sub> conformers after matching the positions of UBE2D2 is increased to  $1.81 \pm 0.46$  Å.

### RING<sub>MUL1</sub> induced CSP in the wider regions of <sup>15</sup>N-UBE2D2

Based on the complex structures, we examined the interaction between RING<sub>MUL1</sub> and UBE2D2 using CSP experiments. The HSQC spectrum of <sup>15</sup>N-RING<sub>MUL1</sub> exhibited high heterogeneity in the presence of only half-molar UBE2D2 and many peaks disappeared (Fig. 2E and Fig. S1A), and many HSQC crosspeaks of <sup>15</sup>N-UBE2D2 also disappeared in the presence of RING<sub>MUL1</sub> (Fig. 2F and Fig. S1B), which were likely correlated with the positional plasticity of the crystal structures of RING<sub>MUL1</sub> and UBE2D2 (Fig. 2A). It has been reported that the allosteric effect of the non-covalent binding of UB (UB<sub>BS</sub>) to the backside of UBE2D2 ( $\alpha$ 1-to- $\beta$ 2; Fig. 1J, bottom region) increases the binding affinity of RING<sub>RNF38</sub> to UBE2D2<sup>S</sup>-UB<sub>OE</sub>, and not to UBE2D2 ( $K_d$ , 89, 73, 4.6, and 0.36  $\mu$ M for UBE2D2, UBE2D2:UB<sub>BS</sub>, UBE2D2<sup>S</sup>-UB<sub>OE</sub>, and UBE2D2<sup>S</sup>-UB<sub>OE</sub>:UB<sub>BS</sub>, respectively). Moreover, it also increases the intrinsic lysine reactivity of UBE2D2~UB [16]. Interestingly, the RING<sub>MUL1</sub>-binding induced strong CSPs in the regions of <sup>15</sup>N-UBE2D2 ( $\alpha$ 1-to- $\beta$ 2;  $\alpha$ 2-to-the crossover  $\alpha$ 3), which were evidently distant from the direct RING<sub>MUL1</sub>-interacting regions (Fig. 2G) and were used for binding with UB<sub>BS</sub> and UB<sub>D</sub>.

L306 of RING<sub>MUL1</sub> fits in the cleft formed by  $\alpha$ 1 (R5, K8, E9, D12) and the N-terminal  $\alpha$ 3 (T98) of

UBE2D2 (Fig. 2G, inset), which may define the molecular basis of the occurrence of higher amounts of CSPs of UBE2D2 induced by the RING<sub>MUL1</sub>-binding along with the positional plasticity of RING<sub>MUL1</sub> in the complex. The corresponding residues of other RING<sub>E3</sub> domains are mostly conserved as Leu (4auq, RING<sub>BIRC7</sub>; 5d1k, RING<sub>RNF25</sub>; 5ulh, RING<sub>RNF165</sub>; 5fel, RING<sub>TRIM25</sub>; 5d0m, RING<sub>ARK2C</sub>; and 4pql, RING<sub>RNF146</sub>), Ile (6w9d, RING<sub>RNF12</sub>), and Met (6hpr, RING<sub>CLAP1</sub>; 3eb6, RING<sub>CLAP2</sub>; 4v3k, RING<sub>RNF4</sub>; 4ap4, RING<sub>RNF38</sub>), although these residues are changed to Cys (2yho, RING<sub>IDOL</sub>), Ala (1fbv, RING<sub>CBL</sub>), Gln (5mnj, RING<sub>MDM2</sub>), and Glu (5vzw, RING<sub>TRIM23</sub>) at certain instances. The molecular mechanism underlying the activity of UB<sub>BS</sub> remains unclear [17], and the finding that RING<sub>MUL1</sub> induces the exceptionally high levels of CSPs in the regions for inter- and intra-molecular binding of UB<sub>BS</sub> and UB<sub>D</sub> supports the hypothesis that the binding of UB<sub>BS</sub>, UB<sub>D</sub>, and RING<sub>MUL1</sub> to UBE2D2 is linked allosterically.

The disappeared HSQC crosspeaks in the CSP experiments of UBE2D2 and RING<sub>MUL1</sub> are likely dependent on intermediate binding exchange of the NMR time scale ( $K_d$ ,  $\sim 1$   $\mu$ M), resulting in peak-broadenings. Both the HSQC spectra of <sup>15</sup>N-UBE2D3 and <sup>15</sup>N-UBE2D3<sup>RS</sup>-UB<sub>OE</sub> could be traceable in the presence of E4BU [15], and the extensive peak disappearance observed in the case of RING<sub>MUL1</sub> was not noted. Through isothermal titration calorimetry (ITC) measurements, we determined the binding affinity to explain the reason for the larger CSP of UBE2D2 in the presence of RING<sub>MUL1</sub>. The affinity of RING<sub>MUL1</sub> for UBE2D2 was relatively weaker ( $K_d$ ,  $28 \pm 15$   $\mu$ M) than the expected one (Table 1 and Fig. S2), since a binding event of this  $K_d$  value likely causes a CS change during the CSP experiments. The binding of RING<sub>MUL1</sub> and UBE2D2 was an endothermic reaction ( $\Delta H$ ,  $1497 \pm 906$  cal·mol<sup>-1</sup>; Table 1), and thus the formation of RING<sub>MUL1</sub>:UBE2D2 should be entropy-driven to accomplish the negative Gibbs free energy ( $\Delta G = \Delta H - T\Delta S$ ). The  $K_d$  value of RING<sub>MUL1</sub>:UBE2D2 is still lower than those of the other RING/U-box:E2 interactions characterized by NMR experiments (E4BU:UBE2D3<sup>RS</sup>, 97  $\mu$ M; RING<sub>BIRC7</sub>:UBE2D2, too weak; RING<sub>BIRC7</sub>:UBE2D2<sup>S</sup>-UB<sub>OE</sub>, 136  $\mu$ M) [15,18]. The higher binding affinity for UBE2D2 in addition to the positional plasticity of RING<sub>MUL1</sub> causes the apparent CSPs in large areas of UBE2D2. UBE2D2 might have an intrinsic dynamic motion in this area, and the RING<sub>MUL1</sub>-binding selects a specific conformation resulting in the CSP on a large area of UBE2D2. However, no clear relaxation

dispersion curve supporting the presence of an exchanging motion of  $\mu$ s–ms time scale was identified in the extreme CPMG experiment [19] of <sup>15</sup>N-UBE2D2 alone (not shown). Therefore, the large area CSP of UBE2D2 induced by the RING<sub>MUL1</sub>-binding does not seem to be dependent on the conformational selection mechanism of UBE2D2 itself.

### Characterization of the RING<sub>MUL1</sub>:UBE2D2~UB mimetics

Prior to investigation on the binding of RING<sub>MUL1</sub>:UBE2D2 and RING<sub>MUL1</sub>:UBE2D2~UB mimetics to TAD<sub>p53</sub>, we first characterized the stable mimetics of UBE2D2~UB, such as UBE2D2~UB<sub>OE</sub> or UBE2D2~UB isopeptide (UBE2D2~UB<sub>IP</sub>) by HSQC experiments. Since UBE2G1<sup>C90S</sup>-UB<sub>OE</sub> synthesizes K48-linked di-UB even though its activity is lower than that of the thioester [20], UBE2D2<sup>C85S</sup> (UBE2D2<sup>S</sup>)-UB<sub>OE</sub> seems to be an active mimetic of UBE2D2~UB. Therefore, UB<sup>K48R</sup>, and not wild-type UB, was used to synthesize stable mimetics via E1-mediated conjugation. UBE2D2<sup>S22R</sup> (UBE2D2<sup>R</sup>) was used to disrupt the inter-molecular interaction between the attached UB<sub>D</sub> and the backside of different UBE2D2 molecules [21]. To further increase the sensitivity of HSQC experiments, <sup>2</sup>H/<sup>13</sup>C/<sup>15</sup>N-labelled UB<sup>K48R</sup> (<sup>DCN</sup>UB<sup>R</sup>) instead of <sup>15</sup>N-labelled UB<sup>K48R</sup> (<sup>15</sup>NUB<sup>R</sup>) was used for the enzymatic conjugation.

The HSQC spectrum of UBE2D2<sup>S22R/C85S</sup> (UBE2D2<sup>RS</sup>)-<sup>DCN</sup>UB<sup>R</sup><sub>OE</sub> was similar to that of free <sup>DCN</sup>UB<sup>R</sup>, except for the C-terminal residues of UB (Figs 3A and 4A). UBE2D2<sup>RS-DCN</sup>UB<sup>R</sup><sub>OE</sub> alone was stable in buffer solution (pH 6.5), and no apparent hydrolysis was detected after performing the HNCA experiment at 5 °C. However, the addition of RING<sub>MUL1</sub> extensively destabilized UBE2D2<sup>RS-DCN</sup>UB<sup>R</sup><sub>OE</sub>, which prevented the acquisition of one clean HSQC spectrum at 25 °C. The half-life of UBE2D2<sup>RS-DCN</sup>UB<sup>R</sup><sub>OE</sub> in the presence of RING<sub>MUL1</sub> was estimated to be ~1.7 h, and it increased to ~10 h at 5 °C (Fig. 5). This half-life was considerably less than those previously reported for the complexes of E4B minimal U-Box and UbcH5c<sup>C85S</sup>-UB oxyester (E4BU:UBE2D3<sup>S</sup>-UB<sub>OE</sub>; 10 h at pH 5.75 and 20 °C) [15], RING<sub>BIRC7</sub>:UBE2D2<sup>S</sup>-UB<sub>OE</sub> (hydrolysis after 1–3 days at pH 7.0 and 4 °C) [18], and UBE2G1<sup>C90S-DCN</sup>UB<sub>OE</sub> (8.8 h at pH 7.0 and 25 °C), in which the acidic loop of UBE2G1 mimics the effect of the RING<sub>E3</sub> domain [20].

Since the isopeptide bond between K85 of UBE2D2 and G76 of UB is believed to be more stable than that of the oxyester, UBE2D2<sup>RK-DCN</sup>UB<sup>R</sup><sub>IP</sub> was

prepared following the previously reported method [22]. Although UBE2D2<sup>RK-DCN</sup>UB<sup>R</sup><sub>IP</sub> was initially thought to be weakly hydrolysed in the presence of RING<sub>MUL1</sub>, it was confirmed later to be stable using the SDS/PAGE analysis (Fig. 5). We also prepared UBE2D2<sup>RAS-DCN</sup>UB<sub>OE</sub>; the conserved N77 of UBE2D2 that is located near the active C85 residue, stabilizes the oxyanion intermediate during ubiquitylation [23]. The N77A mutation apparently increased the stability of UBE2D2<sup>RAS-DCN</sup>UB<sup>R</sup><sub>OE</sub>, and any HSQC crosspeak of free <sup>DCN</sup>UB<sup>R</sup> was not detected during NMR experiments with RING<sub>MUL1</sub>, RING<sub>MUL1</sub>:AD39, and RING<sub>MUL1</sub>:TAD<sub>p53</sub>. Since UBE2D2<sup>RK-DCN</sup>UB<sup>R</sup><sub>IP</sub> displayed a lower response to the binding of RING<sub>MUL1</sub> and AD39 compared to UBE2D2<sup>RS-DCN</sup>UB<sup>R</sup><sub>OE</sub> likely due to the different geometry between the isopeptide and oxyester (Fig. 6A vs Fig. 3B,C), we focused on UBE2D2<sup>RS-DCN</sup>UB<sup>R</sup><sub>OE</sub> and UBE2D2<sup>RAS-DCN</sup>UB<sub>OE</sub> as active and stable mimetics, respectively, for further studies to evaluate their detailed binding modes for RING<sub>MUL1</sub> and TAD<sub>p53</sub>.

### UBE2D2<sup>RS</sup>-UB<sub>OE</sub> was different from UBE2D2<sup>RAS</sup>-UB<sub>OE</sub> in terms of closed conformation and interactions with RING<sub>MUL1</sub> and TAD<sub>p53</sub>

We measured each clean HSQC spectrum of UBE2D2<sup>RS-DCN</sup>UB<sup>R</sup><sub>OE</sub> in the presence of RING<sub>MUL1</sub> and RING<sub>MUL1</sub>:AD39 at 5 °C. The HSQC spectra of UBE2D2<sup>RS-DCN</sup>UB<sup>R</sup><sub>OE</sub> and free <sup>DCN</sup>UB<sup>R</sup> showed that the UB<sub>D</sub> exhibited less intramolecular interactions with UBE2D2<sup>RS</sup> and favoured an open conformation (Figs 3A and 4A), as previously shown in UBE2D3<sup>RS-15N</sup>UB<sub>OE</sub> [24]. RING<sub>E3</sub> activates E2~UB in a closed conformation and renders the nucleophilic attack by a Lys residue of a target protein [25]. The UB<sub>D</sub> of UBE2D2<sup>RS-DCN</sup>UB<sup>R</sup><sub>OE</sub> likely assumed a closed conformation in the presence of RING<sub>MUL1</sub> (Figs 3B and 4B). The binding exchange kinetics of UB<sub>D</sub> seemed to shift from a fast (weak binding, CS-moving) to an intermediate (stronger binding, disappearance of peak due to line-broadening) NMR time scale. It has been well known that the residues 6–14 and 41–50 of UB<sub>D</sub> play an important role in switching to a closed conformation via an intramolecular interaction with E2 proteins [15,24,26]. Additionally, the RING<sub>MUL1</sub>-binding caused extreme peak-broadening of the C-terminal part of <sup>DCN</sup>UB<sub>D</sub> (residues 70–76; Figs 3B and 4B).

Unexpectedly, the HSQC spectrum of UBE2D2<sup>RAS-DCN</sup>UB<sup>R</sup><sub>OE</sub> showed that its UB<sub>D</sub> already adapted to a more closed conformation even in the absence of RING<sub>MUL1</sub> (Fig. 3D). The scale of the

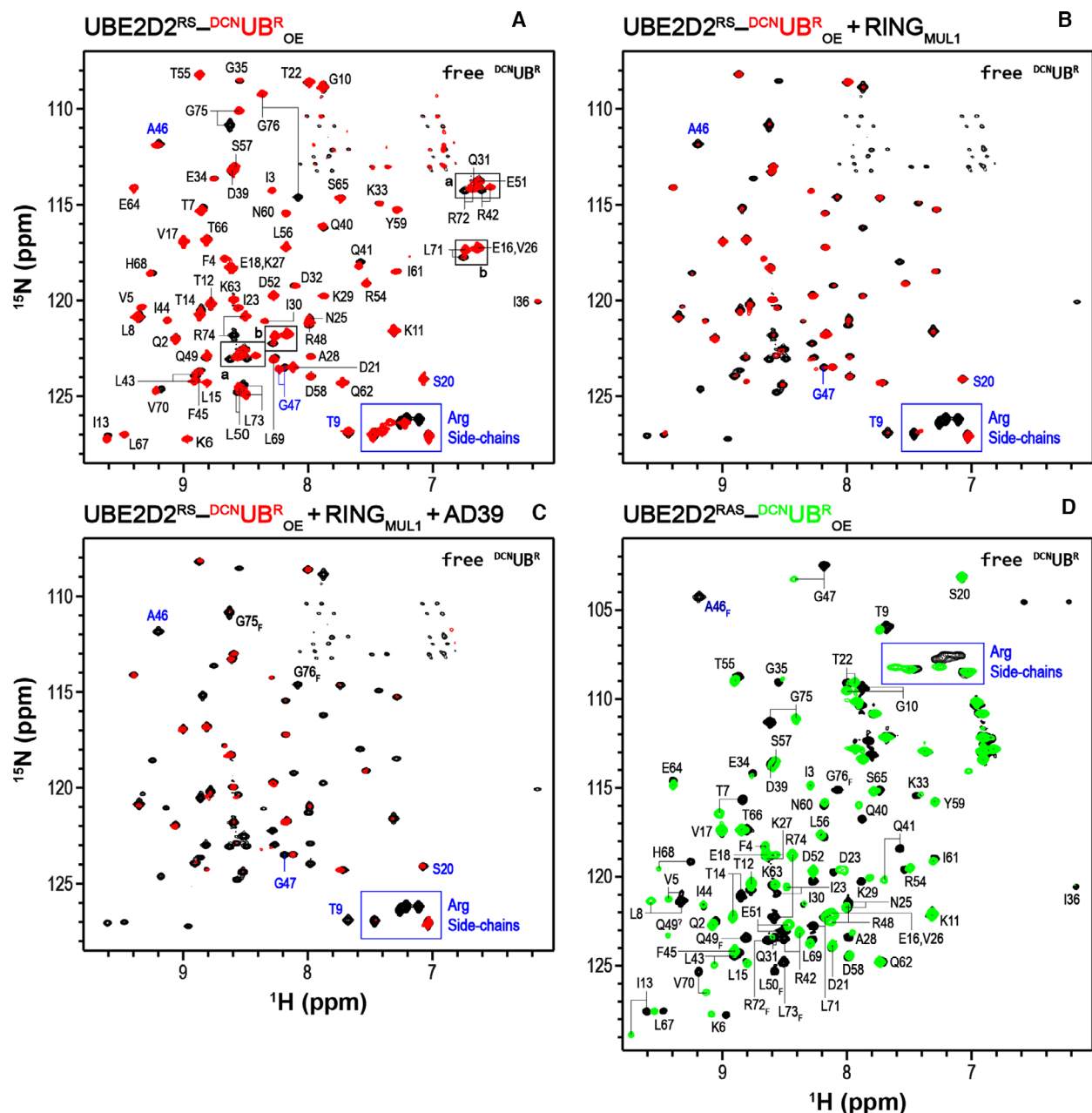


**Fig. 3.** Monitoring the attached UB<sub>D</sub> of UBE2D2<sup>RS\_DCN</sup>UB<sup>R</sup><sub>OE</sub> and UBE2D2<sup>RAS\_DCN</sup>UB<sup>R</sup><sub>OE</sub> via <sup>1</sup>H-<sup>15</sup>N HSQC experiments. All NMR experiments were performed at 5 °C, and the HSQC spectra were overlaid to that of free <sup>DCN</sup>UB<sup>R</sup> (black). The <sup>1</sup>H-<sup>15</sup>N TROSY-HSQC spectra of 0.1 mM UBE2D2<sup>RS\_DCN</sup>UB<sup>R</sup><sub>OE</sub> (A), RING<sub>MUL1</sub>:UBE2D2<sup>RS\_DCN</sup>UB<sup>R</sup><sub>OE</sub> (1:1) (B), and RING<sub>MUL1</sub>:UBE2D2<sup>RS\_DCN</sup>UB<sup>R</sup><sub>OE</sub>:AD39 (1:1:2) (C) were recorded with the reduced <sup>15</sup>N-dimension to decrease the acquisition time. (D) The HSQC spectrum of 0.1 mM UBE2D2<sup>RAS\_DCN</sup>UB<sup>R</sup><sub>OE</sub> shows that the N77A mutation of UBE2D2 considerably affects the conformation of UB<sub>D</sub> in the absence of RING<sub>MUL1</sub>. The folded peaks are indicated with blue letters. When the peaks of free <sup>DCN</sup>UB<sup>R</sup> are only visible, these are indicated with the subscript F.

CSPs (Fig. 4D) was considerably higher than those of UBE2D2<sup>RS\_DCN</sup>UB<sup>R</sup><sub>OE</sub> (Fig. 4A) and RING<sub>MUL1</sub>:UBE2D2<sup>RS\_DCN</sup>UB<sup>R</sup><sub>OE</sub> (Fig. 4B). The N77 residue of UBE2D2 can form a hydrogen bond with the G76 carbonyl group of the attached UB<sub>D</sub>, and it was clear

that the presence of N77 inhibited the formation of a closed conformation of UB<sub>D</sub>. Since UBE2D2<sup>RAS\_DCN</sup>UB<sup>R</sup><sub>OE</sub> already adopted a closed conformation, the RING<sub>MUL1</sub>-binding only caused a marginal CSP of <sup>DCN</sup>UB<sup>R</sup><sub>D</sub> (Figs 4E and 6B). Moreover, the



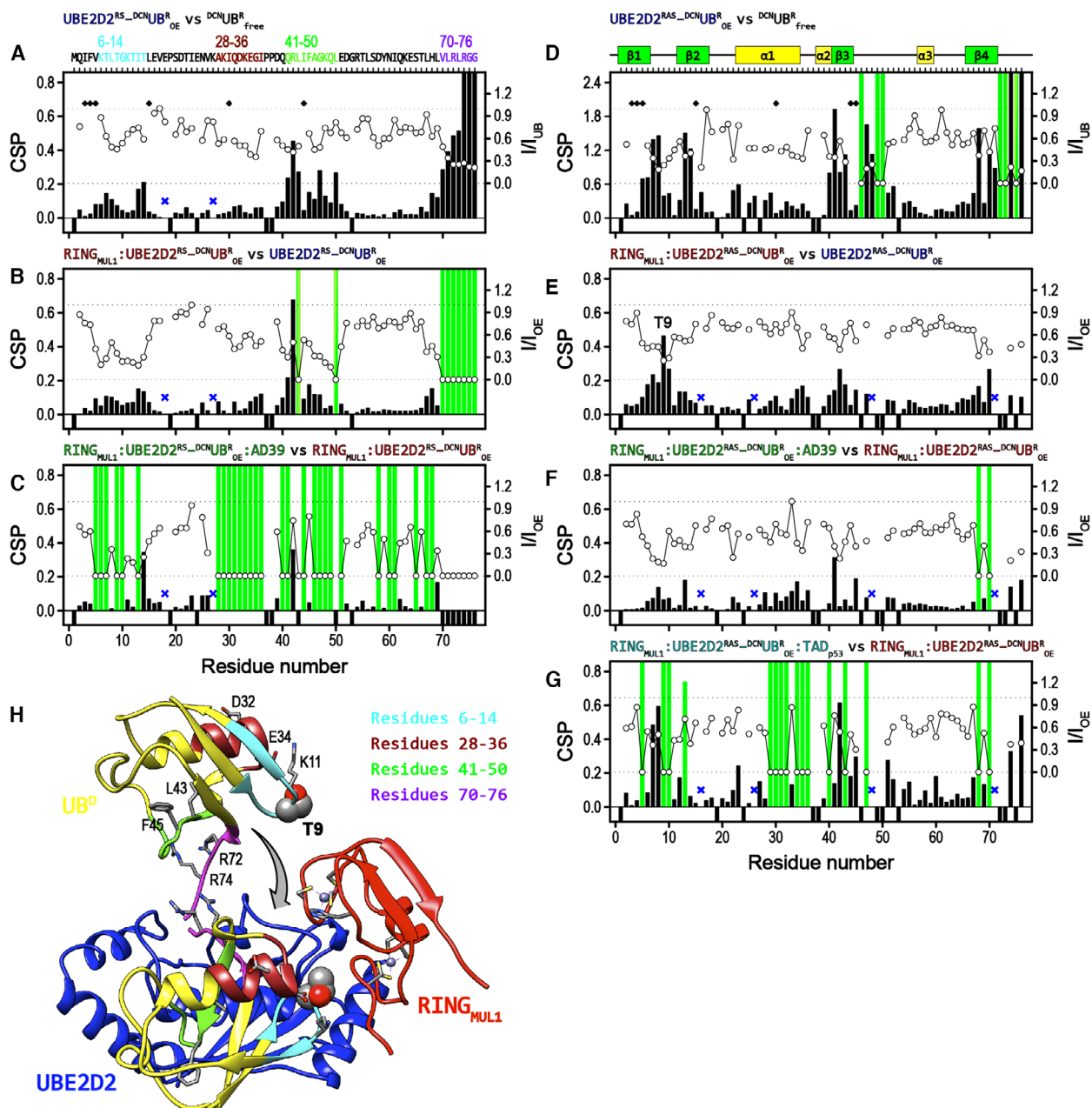


**Fig. 4.** Monitoring the UB<sub>D</sub> conformation in UBE2D2<sup>RS\_DCN</sup>UB<sup>R</sup><sub>OE</sub> and UBE2D2<sup>RAS\_DCN</sup>UB<sup>R</sup><sub>OE</sub> complexes by the HSQC experiments. The CSPs of UBE2D2<sup>RS\_DCN</sup>UB<sup>R</sup><sub>OE</sub> (A–C) and UBE2D2<sup>RAS\_DCN</sup>UB<sup>R</sup><sub>OE</sub> (D–G) in the absence and presence of interacting counterparts. The residues corresponding to the <sup>1</sup>H–<sup>15</sup>N HSQC crosspeaks that were not accurately traced due to the absence of peaks and that disappeared during the CSP experiments are indicated with negative and green bars, respectively. The residues with the intensity ratios ( $I_{UB}$ ) higher than 1.5 are indicated with plus symbols. The residues for which CSP analysis was difficult due to the peak overlap are indicated with blue cross symbols. (H) Ribbon models of the open and closed forms of UBE2D2–UB<sub>D</sub>, in which the closed model was obtained by combining two structures of our RING<sub>MUL1</sub>:UBE2D2 and RING<sub>BIRC7</sub>:UBE2D1<sup>RAS</sup>–UB<sub>D</sub> (PDB, 4auq). The specific regions of UB<sub>D</sub> are indicated with different colours, and the T7 residue of UB<sub>D</sub> is indicated by spheres.

RING<sub>MUL1</sub>-binding also resulted in the different CSP pattern of UBE2D2<sup>RAS\_DCN</sup>UB<sup>R</sup><sub>OE</sub> from that of UBE2D2<sup>RS\_DCN</sup>UB<sup>R</sup><sub>OE</sub>. The CSPs of UBE2D2<sup>RS\_DCN</sup>UB<sup>R</sup><sub>OE</sub> mainly occurred in residues 41–50 of UB<sub>D</sub>

(Fig. 4B,H), whereas those of UBE2D2<sup>RAS\_DCN</sup>UB<sup>R</sup><sub>OE</sub> mainly occurred in residues 6–14, including T9 located near the bound RING<sub>MUL1</sub> (Fig. 4E,H). The model structures of RING<sub>MUL1</sub>:UBE2D2<sup>RS</sup>–UB<sup>R</sup><sub>OE</sub>

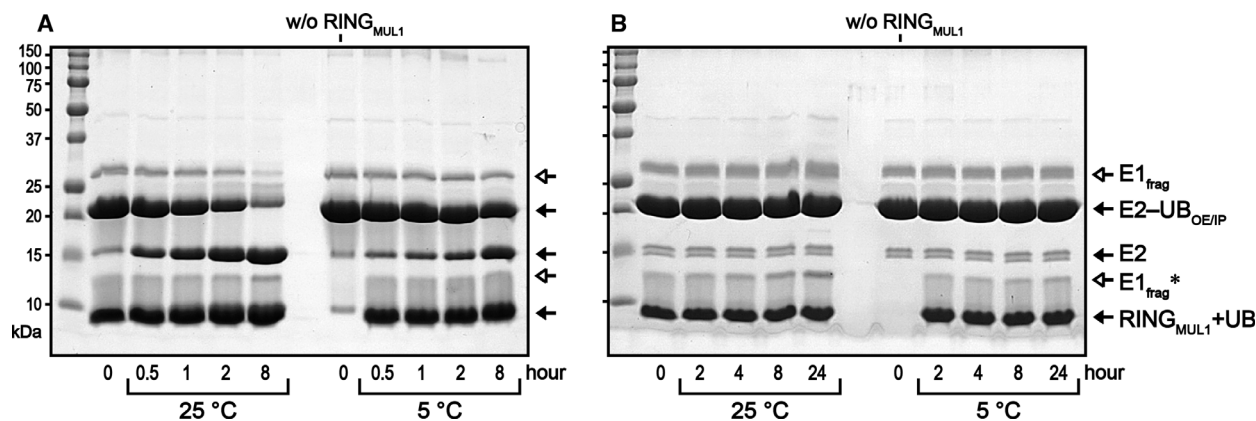


**Fig. 5.** The estimation of stabilities of (A) UBE2D2<sup>RS\_DCN</sup>UB<sup>R\_OE</sup> and (B) UBE2D2<sup>RK\_DCN</sup>UB<sup>R\_IP</sup> in the presence of RING<sub>MUL1</sub>. The hydrolyses of UBE2D2<sup>RS\_DCN</sup>UB<sup>R\_OE</sup> and UBE2D2<sup>RK\_DCN</sup>UB<sup>R\_IP</sup> were assessed by SDS/PAGE analysis. A small amount of E1 fragments (E1<sub>frag</sub> and E1<sub>frag</sub>\*) remained after the purification of UBE2D2-UB mimetics. The hydrolysis of UBE2D2<sup>RS\_DCN</sup>UB<sup>R\_OE</sup> was greatly enhanced by the RING<sub>MUL1</sub>-binding, but that of UBE2D2<sup>RK\_DCN</sup>UB<sup>R\_IP</sup> was not. The half-lives of UBE2D2<sup>RS\_DCN</sup>UB<sup>R\_OE</sup> were  $1.67 \pm 0.02$  and  $10.3 \pm 1.1$  h at 25 and 5 °C, respectively.

was generated via energy minimization of the hybrid model from two PDB coordinates of our RING<sub>MUL1</sub>:UBE2D2 and RING<sub>BRIC7</sub>:UBE2D2<sup>RAS</sup>-UB<sup>R\_OE</sup> (PDB, 4auq). The 2D HSQC spectra for UBE2D2<sup>RAS\_DCN</sup>UB<sup>R\_OE</sup> and free <sup>DCN</sup>UB<sup>R</sup> differ in terms of both CSP and peak intensity (Figs 3D and 4D), but those for UBE2D2<sup>RS\_DCN</sup>UB<sup>R\_OE</sup> and RING<sub>MUL1</sub>:UBE2D2<sup>RS\_DCN</sup>UB<sup>R\_OE</sup> differ mostly in peak intensity (Figs 3B and 4B).

The presence of AD39 resulted in the disappearance of the many HSQC crosspeaks of RING<sub>MUL1</sub>:UBE2D2<sup>RS\_DCN</sup>UB<sup>R\_OE</sup> (Figs 3C and 4C). The CSPs of RING<sub>MUL1</sub>:UBE2D2<sup>RAS\_DCN</sup>UB<sup>R\_OE</sup> induced by the AD39-binding (Fig. 4F) were much less than those of RING<sub>MUL1</sub>:UBE2D2<sup>RS\_DCN</sup>UB<sup>R\_OE</sup> (Fig. 4C). However, the binding of TAD<sub>p53</sub> resulted in higher CSP levels of RING<sub>MUL1</sub>:UBE2D2<sup>RAS\_DCN</sup>UB<sup>R\_OE</sup> (Fig. 4G), and the HSQC spectrum (Fig. 6B) showed increased similarity with that of RING<sub>MUL1</sub>:UBE2D2<sup>RS\_DCN</sup>UB<sup>R\_OE</sup>:AD39 (Fig. 3C).

#### RING<sub>MUL1</sub>:UBE2D2<sup>RAS\_DCN</sup>UB<sup>R\_OE</sup> exhibits an enhanced binding affinity for TAD<sub>p53</sub> compared to UBE2D2:RING<sub>MUL1</sub>

The  $K_d$  values between RING<sub>MUL1</sub>:UBE2D2 and TAD<sub>p53</sub> ( $171 \pm 38$  μM) was estimated by the CSP experiments with <sup>15</sup>N-TAD<sub>p53</sub> as increasing the concentration of RING<sub>MUL1</sub>:UBE2D2, in which the HSQC peaks of the AD49 region were traced (Table 1). Similar binding affinities of TAD<sub>p53</sub> and AD39 for RING<sub>MUL1</sub>:UBE2D2 ( $111 \pm 31$  and  $184 \pm 13$  μM, respectively) were also confirmed via ITC experiments (Table 1 and Fig. S2). Interestingly, the  $\Delta H$  value of the binding between

RING<sub>MUL1</sub>:UBE2D2 and TAD<sub>p53</sub> ( $-673$  kcal·mol<sup>-1</sup>) was higher than that between RING<sub>MUL1</sub>:UBE2D2 and AD39 ( $-1134$  kcal·mol<sup>-1</sup>). Thus, the higher binding affinity of TAD<sub>p53</sub> to RING<sub>MUL1</sub>:UBE2D2 compared to that observed with AD39 was attributed to more entropic contribution ( $-T\Delta S$ ) arising from the SN15 region.

Although UBE2D2<sup>RAS</sup>-UB<sup>R\_OE</sup> did not seem to be identical to UBE2D2<sup>RS</sup>-UB<sup>R\_OE</sup>, it was used to study the binding thermodynamics of RING<sub>MUL1</sub> and TAD<sub>p53</sub> due to its high stability in solution. The CSPs of <sup>15</sup>N-TAD<sub>p53</sub> in the presence of RING<sub>MUL1</sub>:UBE2D2<sup>RAS</sup>-UB<sup>R\_OE</sup> showed that the interaction region of TAD<sub>p53</sub>, which was centred on a specific part of AD39, including W53 and F54, was propagated over whole regions from AD39 to SN15 (Fig. 1C,D). Therefore, the AD39 region seemed to be primarily recognized by the RING<sub>MUL1</sub>:UBE2D2<sup>RAS</sup>-UB<sup>R\_OE</sup>. The 2D HSQC crosspeaks of the AD39 region specifically disappeared as increasing the concentration of RING<sub>MUL1</sub>:UBE2D2<sup>RAS</sup>-UB<sup>R\_OE</sup>, and thus the  $K_d$  values of RING<sub>MUL1</sub>:UBE2D2<sup>RAS</sup>-UB<sup>R\_OE</sup> for AD39 and for TAD<sub>p53</sub> were determined to be  $129 \pm 22$  μM and  $34 \pm 16$  μM, respectively, via ITC experiments (Table 1 and Fig. S2). The molecular basis of  $\Delta S$  contribution to the binding  $\Delta G$  was difficult to be inferred, but the 4-times higher binding affinity of TAD<sub>p53</sub> for RING<sub>MUL1</sub>:UBE2D2<sup>RAS</sup>-UB<sup>R\_OE</sup>, compared to that of AD39, was attributed to the SN15 region ( $\Delta H$ ,  $-629$  and  $485$  kcal·mol<sup>-1</sup>;  $\Delta S$ ,  $15.7$  and  $20.6$  cal·mol<sup>-1</sup>·deg<sup>-1</sup> for AD39 and TAD<sub>p53</sub>, respectively).

The AD39 region of TAD<sub>p53</sub> reportedly forms an induced  $\alpha$ -helical structure when binding to Bcl-X<sub>L</sub> [27] and MDM2 [28]. We examined whether the secondary structure of AD39 was changed in the presence

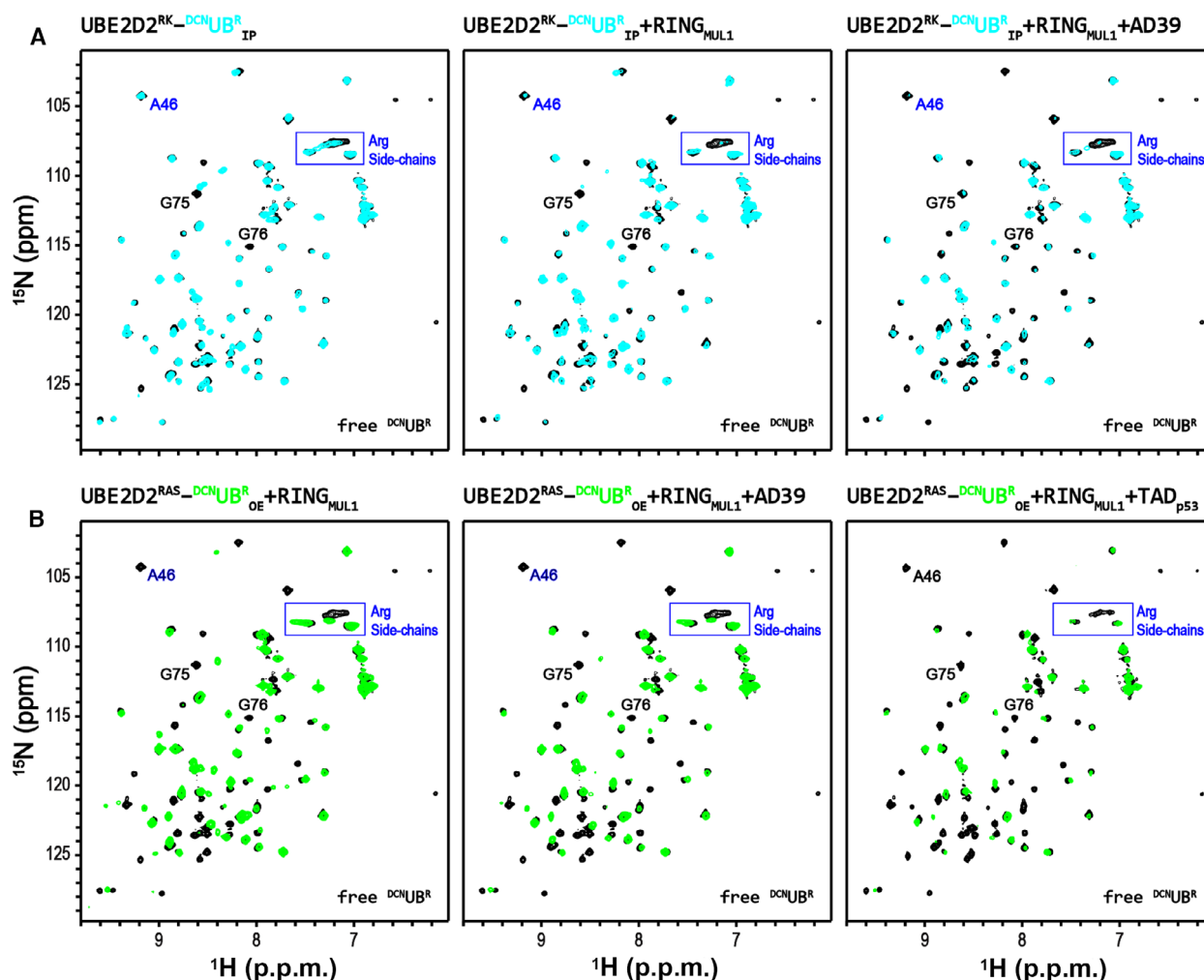


**Fig. 6.** The  $^1\text{H}$ - $^{15}\text{N}$  HSQC spectra of UBE2D2<sup>RK-DCN</sup>UB<sup>R</sup><sub>IP</sub> (A) and UBE2D2<sup>RAS-DCN</sup>UB<sup>R</sup><sub>OE</sub> (B). The folded peaks are indicated with blue letters. The HSQC spectra of 0.1 mM UBE2D2<sup>RK-DCN</sup>UB<sup>R</sup><sub>IP</sub> and 0.1 mM UBE2D2<sup>RAS-DCN</sup>UB<sup>R</sup><sub>OE</sub> were recorded at 5 °C, in the absence and presence of the interacting counterparts. The used concentrations of RING<sub>MUL1</sub>, AD39, and TAD<sub>p53</sub> were 0.1, 0.2, and 0.2 mM, respectively. The HSQC spectrum of UBE2D2<sup>RK-DCN</sup>UB<sup>R</sup><sub>IP</sub> was similar to that of UBE2D2<sup>RS-DCN</sup>UB<sup>R</sup><sub>OE</sub> (Fig. 3A); however, changes in its spectra, induced by the binding of RING<sub>MUL1</sub> and RING<sub>MUL1</sub>:AD39, were less than those of UBE2D2<sup>RS-DCN</sup>UB<sup>R</sup><sub>OE</sub> (Fig. 3B,C), respectively.

of RING<sub>MUL1</sub>:UBE2D2<sup>RAS</sup>-UB<sup>R</sup><sub>OE</sub> via circular dichroism (CD) spectroscopy. The  $K_d$  value of 129  $\mu\text{M}$  (Table 1) assumed that  $\sim 0.45$  fraction of the AD39 bound the RING<sub>MUL1</sub>:UBE2D2<sup>RAS</sup>-UB<sup>R</sup><sub>OE</sub>. However, no increased formation of an  $\alpha$ -helical structure was identified (Fig. 7). It is likely that TAD<sub>p53</sub> binds RING<sub>MUL1</sub>:UBE2D2~UB without the formation of any defined secondary structure.

#### The increased binding affinity of RING<sub>MUL1</sub>:UBE2D2~UB<sub>OE</sub> for TAD<sub>p53</sub> depends on multivalent interactions

Tracing of TAD<sub>p53</sub>-binding surfaces via CSP experiments using  $^{15}\text{N}$ UBE2D2 and  $^{15}\text{N}$ RING<sub>MUL1</sub> even in

the context of stable RING<sub>MUL1</sub>:UBE2D2<sup>RAS</sup>-UB<sup>R</sup><sub>OE</sub> was impossible, since most HSQC peaks of  $^{15}\text{N}$ UBE2D2<sup>RAS</sup> and  $^{15}\text{N}$ RING<sub>MUL1</sub> disappeared in the complexes due to a severe exchange peak-broadening (not shown). Even deuterated RING<sub>MUL1</sub> ( $^{13}\text{C}$ RING<sub>MUL1</sub>) did not result in an analysable HSQC spectrum in the presence of UBE2D2<sup>RAS</sup>-UB<sup>R</sup><sub>OE</sub> (not shown). Therefore, we attempted to map the binding sites for AD39 sequentially using (a) RING<sub>MUL1</sub>: $^{15}\text{N}$ UBE2D2 (Fig. 8A,D, red CSP colour), (b)  $^{15}\text{N}$ RING<sub>MUL1</sub>:UBE2D2 (Fig. 8B,D, blue CSP colour), and (c) RING<sub>MUL1</sub>:UBE2D2<sup>RS-DCN</sup>UB<sup>R</sup><sub>OE</sub> (Figs 4C and 8E), respectively. The hybrid model structure of a closed conformation (Fig. 4H) was used to show the surfaces of the attached UB<sub>D</sub> in RING<sub>MUL1</sub>:UBE2D2-<sup>DCN</sup>UB<sup>R</sup><sub>OE</sub> that bound to AD39.

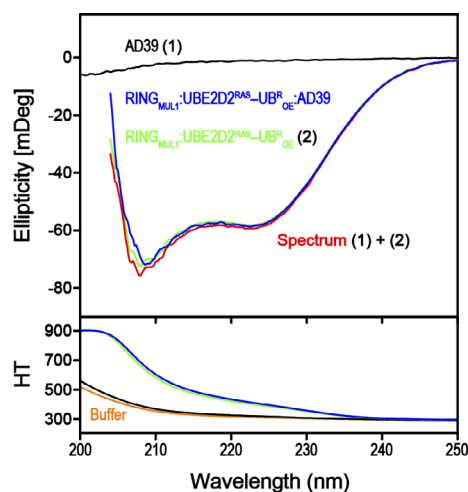


**Fig. 7.** Estimation of the secondary structure of the bound AD39 peptide to UBE2D2<sup>RAS</sup>-UB<sup>R</sup><sub>OE</sub> by CD experiments. The protein samples were prepared in the same NMR buffer (pH 6.5, 50 mM MES, 50 mM NaCl, and 5  $\mu$ M ZnSO<sub>4</sub>) and the CD experiments were performed at room temperature. The CD spectra of each separate 0.1 mM AD39 and RING<sub>MUL1</sub>:UBE2D2<sup>RAS</sup>-UB<sup>R</sup><sub>OE</sub> were recorded and then the spectra were arithmetically added (red). The CD spectrum of the mixed 0.1 mM RING<sub>MUL1</sub>:UBE2D2<sup>RAS</sup>-UB<sup>R</sup><sub>OE</sub>:AD39 was recorded for the comparison (blue). Any increased  $\alpha$ -helical structure of AD39 is not shown in the complex form with RING<sub>MUL1</sub>:UBE2D2<sup>RAS</sup>-UB<sup>R</sup><sub>OE</sub>, since no decrease of CD ellipticity at 222 nm was observed for the mixed sample.

UBE2D2 exhibited the presence of two regions that interacted with AD39, wherein the main region was located in the vicinity of the RING-binding site of UBE2D2 ( $\alpha$ 1 and N-terminal  $\alpha$ 3; Fig. 1F,J), which was also identified in the CSPs of RING<sub>MUL1</sub>:<sup>15</sup>N-UBE2D2 (Fig. 8A,D). The AD39-binding to the main region of UBE2D2 could additionally stabilize the closed conformation of the attached UB<sub>D</sub> by shifting RING<sub>MUL1</sub> close to the UB<sub>D</sub> region of UBE2D2~UB. The CSPs of <sup>15</sup>N-RING<sub>MUL1</sub>:UBE2D2 by AD39 (Fig. 8B) showed that  $\beta$ 1, the unstructured N- and C-terminal regions of <sup>15</sup>N-RING<sub>MUL1</sub> were also perturbed (Fig. 8D, blue CSP colour). The higher amount of CSPs for the same concentration of AD39, compared to <sup>15</sup>N-RING<sub>MUL1</sub> alone (Fig. 8B,C), indicated that the presence of UBE2D2 increased the binding affinity for AD39. Although the CSPs of RING<sub>MUL1</sub>:UBE2D2<sup>RS-DCN</sup>-UB<sup>R</sup><sub>OE</sub> induced upon the AD39-binding were strongly coupled to the exchange motions of UB<sub>D</sub>, which also caused the significant CSPs located in the UBE2D2-contacting region of <sup>DCN</sup>-UB<sup>R</sup><sub>D</sub>, the mapping of the CSPs of RING<sub>MUL1</sub>:UBE2D2<sup>RS-DCN</sup>-UB<sup>R</sup><sub>OE</sub> on the surface model clearly indicated that the interface between RING<sub>MUL1</sub> and UB<sub>D</sub> of RING<sub>MUL1</sub>:UBE2D2<sup>RS-DCN</sup>-UB<sup>R</sup><sub>OE</sub> complex also participated in its interaction with AD39 (Fig. 8E,

marked with a cyan circle). The AD39-binding also caused the CSPs in another surface of UB<sub>D</sub> that is distant from the UBE2D2-binding interface (Fig. 8E, marked with yellow circle). Overall, the interaction of AD39 with RING<sub>MUL1</sub>:UBE2D2<sup>RS-DCN</sup>-UB<sup>R</sup><sub>OE</sub> displayed a multivalency of cumulative weak bindings, which is a typical characteristic of IDP interaction [29].

TAD<sub>p53</sub> resulted in stronger CSPs of RING<sub>MUL1</sub>:UBE2D2<sup>RS-DCN</sup>-UB<sup>R</sup><sub>OE</sub> compared to AD39 (Fig. 4F, G). The occurrence of synergistic interactions by TAD<sub>p53</sub>, from AD39 to SN15, enhanced its binding affinity for RING<sub>MUL1</sub>:UBE2D2<sup>RS-DCN</sup>-UB<sup>R</sup><sub>OE</sub>. The lengths of the extended AD39 region and the long horizontal axis of UBE2D2 were  $\sim$ 65 and  $\sim$ 50 Å (Fig. 1J), respectively, and the binding stoichiometry (N) of RING<sub>MUL1</sub>:UBE2D2<sup>RS-DCN</sup>-UB<sup>R</sup><sub>OE</sub> for TAD<sub>p53</sub> determined by the ITC measurements was close to 1 ( $0.67 \pm 0.19$ ; Table 1). Therefore, TAD<sub>p53</sub> seemed to encompass whole interaction regions involving RING<sub>MUL1</sub>, UBE2D2, and UB<sub>D</sub>.

## Discussion

### Differential characteristics of various UBE2D2~UB mimetics upon RING<sub>MUL1</sub> binding

Closed conformation of E2~UB reportedly plays an important role in the RING-E3-mediated ubiquitylation [15,17,30]. The UB<sub>D</sub> molecules of RING:UBE2D1<sup>RAS</sup>-UB<sub>OE</sub> (PDB, 4auq) and various other RING:E2~UB<sub>IP</sub> complexes (PDB, 4ap4, 4v3k, 5fer, 5mnj, 5vgw, and 6hpr) have the common converged position via the linchpin interactions (Fig. 9A). However, the closed conformation of UB<sub>D</sub> in the recent crystal structure of RING<sub>RNF12</sub>:UBE2D2<sup>RK</sup>-UB<sub>IP</sub> [31] is different from those of the linchpin structures (Fig. 9B). Middleton *et al.* reported that direct contact between the UB<sub>D</sub> and RING<sub>RNF12</sub> was absent, indicating that although UB<sub>D</sub> in RING<sub>RNF12</sub>:E2~UB might possess a range of conformational spaces, locking of UB<sub>D</sub> in the prime conformation via additional intramolecular RING-to-UB<sub>D</sub> linchpin contact could be critical for ubiquitylation [31]. Interestingly, the CSP pattern of UBE2D2<sup>RS-DCN</sup>-UB<sup>R</sup><sub>OE</sub> induced by RING<sub>MUL1</sub> (Fig. 4E) is well matched with the linchpin structure (Fig. 9C), in which the T9 of UB<sub>D</sub> has a close contact with the RING<sub>E3</sub> domains. However, that of UBE2D2<sup>RS-DCN</sup>-UB<sup>R</sup><sub>OE</sub> by RING<sub>MUL1</sub> (Fig. 4B) is correlated with the structure of RING<sub>RNF12</sub>:UBE2D2<sup>RK</sup>-UB<sub>IP</sub> (Fig. 9C). Although the molecular basis for the activation of UBE2D2~UB mediated by the RING<sub>MUL1</sub>-binding remains unknown, a special UBE2D2-binding mechanism

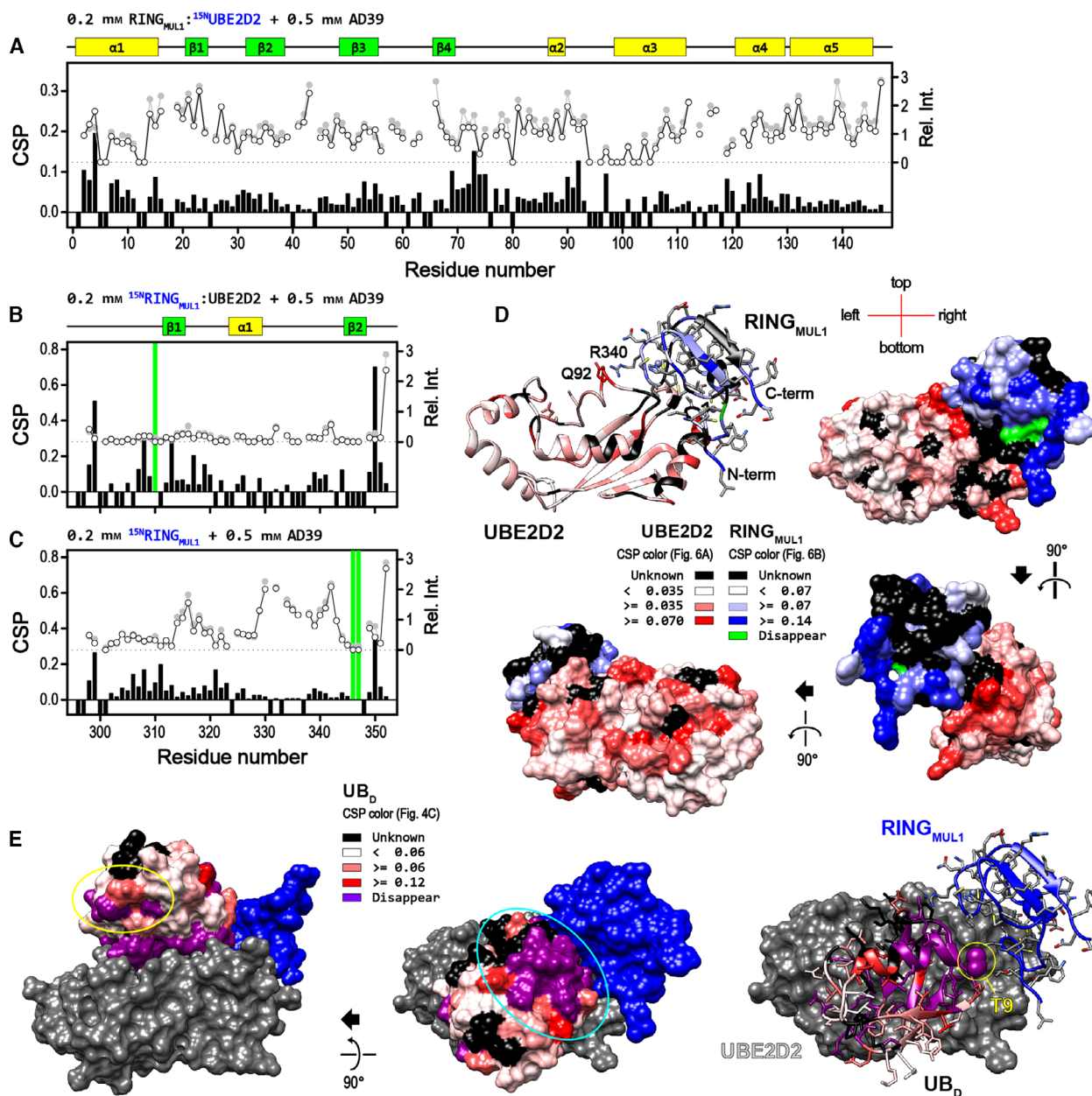


**Fig. 8.** The binding surfaces of RING<sub>MUL1</sub>:UBE2D2 and RING<sub>MUL1</sub>:UBE2D2<sup>RS</sup>-UB<sup>ROE</sup> for AD39. The CSPs of 0.2 mM RING<sub>MUL1</sub>:<sup>15</sup>N-UBE2D2 (A), <sup>15</sup>N-RING<sub>MUL1</sub>:UBE2D2 (B), and <sup>15</sup>N-RING<sub>MUL1</sub> (C) in the presence of 0.5 mM AD39 are shown as bar plots, respectively. The amount of CSPs induced by the AD39-binding is higher in <sup>15</sup>N-RING<sub>MUL1</sub>:UBE2D2 than that in <sup>15</sup>N-RING<sub>MUL1</sub> alone. (D) The CSPs of RING<sub>MUL1</sub>:<sup>15</sup>N-UBE2D2 (panel-A) and <sup>15</sup>N-RING<sub>MUL1</sub>:UBE2D2 (panel-B) induced by the AD39-binding are indicated on the surface model via red and blue tones, respectively. (E) The CSPs of 0.1 mM RING<sub>MUL1</sub>:UBE2D2<sup>RS</sup>-DCN-UB<sup>ROE</sup> by 0.2 mM AD39, as shown in Fig. 4C, are indicated on the surface model of RING<sub>MUL1</sub>:UBE2D2-UB<sub>D</sub>. The AD39-binding also caused the CSPs in the other surfaces of UB<sub>D</sub> that are distant from the UBE2D2-binding interface; (a) the cyan circled area, residues 13–14 and 28–34, (b) the yellow circled area, residues 58–61.

seems to be mediated by RING<sub>MUL1</sub>. It may be postulated that subtle structural changes result in the occurrence of allosterically linked inter- and intra-molecular interactions of RING<sub>MUL1</sub>:UBE2D2-UB<sub>D</sub>, in which one instance among the positional plasticity of the

bound RING<sub>MUL1</sub> favoured the transient structure of UBE2D2, thereby stabilizing a closed conformation conducive for the hydrolysis of the attached UB<sub>D</sub>.

The activation of UBE2D2~UB via a closed conformation of UB<sub>D</sub> induced by the RING<sub>MUL1</sub>-binding

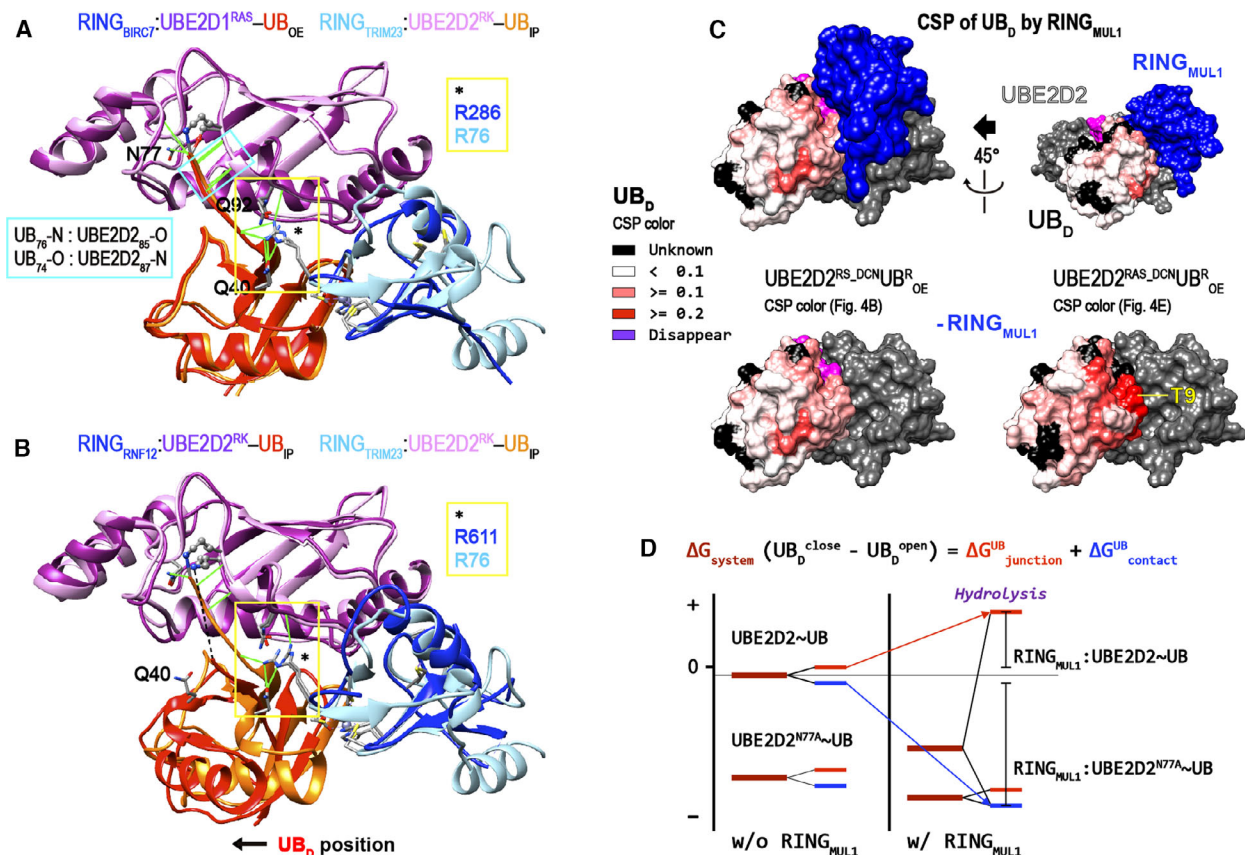


**Fig. 9.** Crystal structures of various RING<sub>E3</sub>:UBE2D2-UB mimetics and the inspection of the N77A mutation effect on a closed conformation. The presence of hydrogen-bonds is indicated with green lines. (A) Representative crystal structures of RING<sub>BIRC7</sub>:UBE2D1<sup>RAS</sup>-UB<sub>OE</sub> and RING<sub>TRIM23</sub>:UBE2D2<sup>RK</sup>-UB<sub>IP</sub> (PDB, [4auq](#) and [5vzw](#)) are superimposed, and the positions of UB<sub>D</sub> are almost identical. (B) The recent crystal structure of RING<sub>RNF12</sub>:UBE2D2<sup>RK</sup>-UB<sub>IP</sub> (PDB, [6w9d](#)) shows that its closed conformation does not have the linchpin structure. (C) The CSPs of UBE2D2<sup>RS\_DCN</sup>UB<sub>OE</sub> (Fig. 4B) and UBE2D2<sup>RAS\_DCN</sup>UB<sub>OE</sub> (Fig. 4E) induced by the RING<sub>MUL1</sub>-binding are decorated on the hybrid model of RING<sub>MUL1</sub>:UBE2D2-UB<sub>OE</sub> using red colour. The CSPs of UB<sub>D</sub> in the side facing the RING<sub>MUL1</sub> are more apparent by the N77A mutation. (D) Gibbs free energy diagram was intuitively illustrated for UBE2D2~UB and UBE2D2<sup>N77A</sup>-UB. Since UBE2D2<sup>RAS\_DCN</sup>UB<sub>OE</sub> already forms a more stable closed conformation, the  $\Delta G_{\text{system}} (\text{UB}_D^{\text{close}} \text{ vs } \text{UB}_D^{\text{open}})$  of UBE2D2<sup>N77A</sup>-UB is markedly lower than that of UBE2D2~UB. When a closed conformation of UB<sub>D</sub> is induced by the RING<sub>MUL1</sub>-binding ( $\Delta G_{\text{contact}}^{\text{UB}}$ ), the presence of N77 can increase the free energy at the junction of UB<sub>D</sub> and UBE2D2 ( $\Delta G_{\text{junction}}^{\text{UB}}$ ). Therefore, the overall  $\Delta G_{\text{system}}$  of RING<sub>MUL1</sub>:UBE2D2~UB is higher than that of RING<sub>MUL1</sub>:UBE2D2<sup>N77A</sup>-UB.

depends critically on the presence of N77. Although detailed characterization of a closed conformation of RING<sub>MUL1</sub>:UBE2D2<sup>RS</sup>-UB<sub>OE</sub> remains further studies, our NMR data showed that the intra- and intermolecular interactions of UBE2D2<sup>RS</sup>-UB<sub>OE</sub> were different from those of UBE2D2<sup>RAS</sup>-UB<sub>OE</sub> in terms of the RING<sub>MUL1</sub>- and TAD<sub>p53</sub>-bindings. To explain the different closed conformations of UBE2D2<sup>RS\_DCN</sup>-UB<sub>OE</sub> and UBE2D2<sup>RAS\_DCN</sup>-UB<sub>OE</sub> conceptually, the Gibbs free energy of the RING<sub>MUL1</sub>-induced closed conformation of UB<sub>D</sub> ( $\Delta G_{\text{system}}$ ) can be divided into the overall contact energy between UBE2D2 and UB<sub>D</sub> ( $\Delta G_{\text{contacts}}^{\text{UB}}$ ) and the local energy at the junction of thioester ( $\Delta G_{\text{junction}}^{\text{UB}}$ ). The high energy state of

$\Delta G_{\text{junction}}^{\text{UB}}$  that activates UBE2D2~UB and is critically dependent on the presence of N77 could be supported by decreasing  $\Delta G_{\text{contacts}}^{\text{UB}}$  relying on the RING<sub>MUL1</sub> binding (Fig. 9D).

### *In vivo* interaction of p53 and RING<sub>MUL1</sub>:E2-UB

The multivalency of TAD<sub>p53</sub> originating from its innate IDP characteristics contributes to its enhanced binding affinity for RING<sub>MUL1</sub>:UBE2D2~UB, which is supported by the estimated binding thermodynamic parameters (Table 1). The formation of the triple complex (RING<sub>MUL1</sub>:UBE2D2~UB) provides additional surfaces for adopting TAD<sub>p53</sub>. TAD<sub>p53</sub> caused the

appreciable CSPs in the various regions of RING<sub>MUL1</sub>:UBE2D2 and RING<sub>MUL1</sub>:UBE2D2<sup>RAS</sup>-UB<sub>OE</sub> (Fig. 8D,E), which is a typical characteristic of the IDP interaction, multivalency [29], and thus the TAD<sub>p53</sub>-binding for RING<sub>MUL1</sub>:UBE2D2<sup>RAS</sup>-UB<sub>OE</sub> is hardly converged to one binding mode. It is likely that the IDP nature of TAD<sub>p53</sub> and its multivalency occurring during binding to RING<sub>MUL1</sub>:UBE2D2~UB may synergistically increase the binding affinity and affect the dynamic nature of UB<sub>D</sub>. The binding stoichiometry (N) between RING<sub>MUL1</sub>:UBE2D2<sup>RAS</sup>-UB<sub>OE</sub> and TAD<sub>p53</sub> is close to 1, and the AD39 region of TAD<sub>p53</sub> is primarily recognized as increasing the size of complexes from RING<sub>MUL1</sub> or UBE2D2 alone to RING<sub>MUL1</sub>:UBE2D2<sup>RAS</sup>-UB<sub>OE</sub>. Therefore, the AD39 region is preferentially located in two interfaces (a) between the  $\alpha 1$  of UBE2D2 and RING<sub>MUL1</sub>, and (b) between UB<sub>D</sub> and RING<sub>MUL1</sub>, and then the SN15 region including K24 faces the accessible junction between UB<sub>D</sub> and UBE2D2, which can render the thioester bond susceptible to the nucleophilic attack by K24.

The measured  $K_d$  values between RING<sub>MUL1</sub>:UBE2D2<sup>RAS</sup>-UB<sub>OE</sub> and TAD<sub>p53</sub> (34  $\mu$ M) may not be sufficient for achieving *in vivo* ubiquitylation of p53 by MUL1. However, native RING<sub>MUL1</sub>:UBE2D2~UB could exhibit a higher affinity for TAD<sub>p53</sub>, since RING<sub>MUL1</sub>:UBE2D2<sup>RS</sup>-UB<sub>OE</sub> displayed a stronger dynamic nature of UB<sub>D</sub> in response to the AD39-binding than that observed with RING<sub>MUL1</sub>:UBE2D2<sup>RAS</sup>-UB<sub>OE</sub>. It is also well documented that the transcription-independent pro-apoptotic function of p53 is associated with stress-induced translocation of p53 to the mitochondria [32–34]. *In vitro* physical interaction between the C-terminal domain of p53 and negatively charged phospholipids has also been reported [35]. Therefore, the reduction in the dimensionality of the interaction from 3D to 2D in the mitochondrial outer membrane may enhance the interaction between MUL1 and p53, thereby facilitating rapid ubiquitylation of the translocated p53 for subsequent processes.

The complex formed by RING<sub>MUL1</sub> with UBE2D2~UB evidently aid the recruitment of TAD<sub>p53</sub> and this ubiquitylation mechanism has not been reported thus far. The *in vivo* regulation and proteostasis of IDPs that are dominantly observed in humans are important for understanding the mechanisms underlying the development of human diseases [29,36]. The ubiquitylation of IDPs could be one of the most commonly observed *in vivo* regulation mechanisms, in which direct recognition of IDPs by other RING<sub>E3</sub>:E2~UB complexes may also be useful.

## Materials and methods

### Protein expression and purification

The human RING<sub>MUL1</sub> domain (residues 298–352), human TAD<sub>p53</sub> (residues 1–73), and UBE2D2 conjugating enzymes were prepared following the previously reported methods [11,14]. Non-tagged UB<sup>K48R</sup> proteins were prepared as per the previously reported method [37]. For the preparation of NMR samples, size exclusion chromatography (SEC) was performed using the NMR-buffer (pH 6.5, 50 mM MES, 50 mM NaCl, 5  $\mu$ M ZnSO<sub>4</sub>, and 1 mM DTT). In the other cases, SEC was performed with a buffer (pH 7.5, 25 mM Tris-HCl, 100 mM NaCl, and 1 mM DTT). The concentrations of all proteins were estimated using their extinction coefficient at 280 nm [38].

For the NMR experiments, the proteins were expressed in M9 minimal media after incubation for 6 h at 30 °C following isopropyl  $\beta$ -D-1-thiogalactopyranoside (IPTG) induction at 0.7–0.8 OD at 600 nm. Isotope-labelled proteins were expressed by growing *Escherichia coli* cells in M9 minimal media (1 L) supplemented with isotope-labelled ammonium chloride (1 g) and glucose (2 g). CELTONE base powder (1 g), vitamins, and trace metals were added to enhance cell growth. All isotope-labelled materials were purchased from Cambridge Isotope Laboratories Inc. The detailed composition of media and the culture method used for protein deuteration are described in previous reports [39].

The mouse E1 gene was cloned into the pRSET-A vector, and then the plasmid was transformed into *E. coli* Rosetta (DE3). The E1 protein was expressed in LB medium for 6 h at 25 °C after IPTG induction at 0.7–0.8 OD at 600 nm. The cultured cells were resuspended in buffer (pH 8.0, 25 mM Tris-HCl, 0.5 M NaCl, 10 mM 2-mercaptoethanol, and 1 mM PMSF). Nonspecific protease activity was reduced by adding EDTA-free protease inhibitor cocktail tablets (Sigma-Aldrich, Seoul, Korea). After cell disruption by sonication, the supernatant was applied to a Histrap HP column (GE Healthcare, Seoul, Korea) as soon as possible. The E1 protein was eluted using 150 ml imidazole gradient with buffer (pH 8.0, 25 mM Tris-HCl, 0.5 M NaCl, 0.5 M imidazole, and 10 mM 2-mercaptoethanol). The protein fractions were dialysed into buffer (pH 8.0, 20 mM Tris-HCl and 1 mM DTT), and then was applied to a Hitrap-Q HP column (GE Healthcare). Elution was performed using a 150 ml NaCl gradient with buffer (pH 8.0, 20 mM Tris-HCl, 1 M NaCl, and 1 mM DTT). The purified E1 protein was concentrated to  $\sim 2.0$  mg·mL<sup>-1</sup>, roughly estimated via SDS/PAGE, and then stored in a –80 °C refrigerator.

### Preparation of the UBE2D2~UB mimetics and estimation of their stabilities in solution

All mimetics, namely, UBE2D2~UB<sub>OE</sub> [20] and UBE2D2~UB<sub>IP</sub> [22], were enzymatically synthesized as previously

reported methods. The mimetics were synthesized via E1-mediated enzymatic reactions of E2 proteins (0.1 mM) in the presence of twice the amount of non-tagged <sup>DCN</sup>UB<sup>R</sup> protein. Briefly, the reactions of UBE2D2<sup>RS</sup> and UBE2D2<sup>RAS</sup> were performed in buffer (pH 9.0, 50 mM CHES, 150 mM NaCl, 1 mM DTT, 4 mM ATP, and 5 mM MgCl<sub>2</sub>) with ~4 μM E1 for 6 h at 35 °C. UBE2D2-UB<sub>IP</sub> was synthesized with ~6 μM E1 in buffer (pH 10.0, 50 mM CAPS, 150 mM NaCl, 1 mM DTT, 4 mM ATP, and 5 mM MgCl<sub>2</sub>) for 24 h at 35 °C. The synthesized UBE2D2~UB mimetics were purified by SEC using the Superdex-75 column in buffer (pH 6.5, 50 mM MES, and 50 mM NaCl).

Each purified 0.1 mM UBE2D2<sup>RS</sup>-UB<sup>ROE</sup> and UBE2D2<sup>RK</sup>-UB<sup>RIP</sup> was incubated with 0.15 mM RING<sub>MUL1</sub> in the NMR-buffer. The reaction mixtures were aliquoted and then were incubated at 25 and 5 °C, respectively. The reaction was stopped at an appropriate time by adding the SDS sample buffer, and then was stored at -20 °C before the SDS/PAGE analysis. The protein bands of UBE2D2-UB mimetics were quantified with the ImageJ program (<https://imagej.nih.gov/ij/>). The half-lives of UBE2D2<sup>RS-DCN</sup>UB<sup>ROE</sup> in the presence of RING<sub>MUL1</sub> were estimated by fitting to the equation of single exponential decay.

### Preparation of peptide samples

SN15 (residues 15–30) and AD39 (residues 39–57) peptides, as well as the colour-dye derivative form of AD39, were purchased from PEPTRON Inc. (Daejeon, Korea). In the dye attached AD39 peptide, the Lys residue coupled to 2,4-dinitrophenyl dye (K-DNP) was attached to the C-terminal of the native form (AMDDLMLSPDDIEQWFTED/K-DNP). All peptides were dissolved in an appropriate experimental buffer, and then an equimolar amount of NaOH as that of the Asp/Glu residues was added to maintain the solution pH value.

### NMR experiments

To assign the backbone CSs of UBE2D2, the HNCACB, HN(CO)CACB, HNCO, and HN(CA)CO spectra were recorded using the Bruker 800 and 900 MHz spectrometers equipped with TCI-cryogenic probe. The HSQC crosspeaks of the mutated proteins (UBE2D2<sup>RS</sup>, UBE2D2<sup>RAS</sup>, UBE2D2<sup>RK</sup>, and UB<sup>R</sup>) and their UB-conjugated forms were assigned by additional HNCA experiments. In the absence of additional comments, NMR experiments were conducted in the NMR buffer (pH 6.5, 50 mM MES, 50 mM NaCl 5 μM ZnSO<sub>4</sub>, and 5% D<sub>2</sub>O) at 25 °C. The CSP data of HSQC peaks were processed using the equation,  $[(6 \times \Delta H)^2 + \Delta N^2]^{1/2}$ , where ΔH and ΔN represent the CS differences of <sup>1</sup>H and <sup>15</sup>N, respectively. Analysis of the protein amide CSs deposited in the Biological Magnetic Resonance Bank (No. 36251) showed that the average distribution of <sup>15</sup>N-CSs was 6-fold greater than that of

<sup>1</sup>H-CSs [40]. All NMR data were processed using the NMRPipe program [41] while spectral analyses were conducted using the NMRFAM-SPARKY program [42].

### Determination of crystal structures of the RING<sub>MUL1</sub> and UBE2D2:RING<sub>MUL1</sub> complex

Detailed crystallization conditions of the RING<sub>MUL1</sub> protein (15 mg·mL<sup>-1</sup>) and the UBE2D2:RING<sub>MUL1</sub> complex (10 mg·mL<sup>-1</sup>) have already been reported [11]. The crystal of UBE2D2 alone was obtained under the conditions of the reservoir buffer containing 0.1 M sodium citrate (pH 5.6), 0.5 M ammonium sulfate, and 1.0 M lithium sulfate during the screening of the UBE2D2:RING<sub>MUL1</sub> crystal. The diffraction data were collected at beamline 7A at the Pohang Accelerator Laboratory, and data were indexed, scaled, and merged using the HKL-2000 software [43].

To solve the structure of RING<sub>MUL1</sub>, we performed molecular replacement (MR) using the Phaser program [44]. Neither the recent NMR ensemble structures of RING<sub>MUL1</sub> (PDB code, 6K2K) nor the homology model calculated using the Phyre2 (Protein Homology/Analogous Recognition Engine) web portal [45] yielded the correct MR results. Therefore, the crystal structure of the UBE2D2:RING<sub>MUL1</sub> complex was solved by MR using the coordinate of UBE2D2 (PDB code, 2ESK), and then the crystal structure of RING<sub>MUL1</sub> alone was solved by MR using the coordinate of RING<sub>MUL1</sub> in the complex. Interactive model building and structure refinement were performed using the Coot program [46] and the PHENIX software suite [47]. The calculated crystal structures were validated using the MolProbity web portal [48].

### Biophysical analyses

All protein samples, except the peptide samples, were prepared using a buffer (pH 6.5, 50 mM MES, 50 mM NaCl, 5 μM ZnSO<sub>4</sub>, and 1 mM TCEP) through dialysis or SEC. ITC experiments were performed using the Auto-iTC200 micro-calorimeter (Malvern Panalytical, Malvern, UK) at 10 °C. The low concentrated protein was loaded in the sample cell, and 15–30 higher concentrated titrant protein was placed in the syringe. ITC data were analysed using the MICROCAL ORIGIN<sup>TM</sup> software.

Circular dichroism spectra were recorded using the J-715 CD instrument (JASCO, Tokyo, Japan) with 0.05 cm path-length circular CD cell to measure high-concentration protein samples (0.1 mM, > 3.0 mg·mL<sup>-1</sup>). All protein and peptide samples were prepared using a buffer (pH 6.5, 50 mM MES, 50 mM NaCl, and 5 μM ZnSO<sub>4</sub>).

### Structure presentations and analyses

Visualizations of all structures were performed using the Chimera program [49]. The CSP data were presented via a



colour gradient using the B-factor column of the PDB files. The RMSD values of the structures were calculated using the AmberTools21 program package (<https://ambermd.org/AmberTools.php>). The evaluation of the RING<sub>MUL1</sub> crystal structures based on the <sup>1</sup>H–<sup>15</sup>N RDC values was done with the calcETensor analysis module of the Xplor-NIH program [50].

## Accession numbers

The PDB coordinates of UBE2D2 (PDB ID: [7BOL](#)), RING<sub>MUL1</sub> (PDB ID: [6M2D](#)), and RING<sub>MUL1</sub>:UBE2D2 (PDB ID: [6M2C](#)) were deposited to protein data bank (PDB).

## Acknowledgements

This work was supported by the KBSI grants (T39632 and C130000) and by the National Research Foundation grants funded by the Korean government (NRF-2017R1E1A1A01074403, NRF-2019M3E5D4069903, and NRF-2019M3A9C4076156). This work was also supported by the KRIBB Research Initiative Program (KGM9952112).

## Conflict of interest

The authors declare no conflict of interest.

## Author contributions

SWC, CKL, and KSR planned this research project. MSL and SOL performed the NMR and X-ray experiments, respectively. JC performed most of the additional experiments. MR, MKL, JHK, and EH were involved in the design and data interpretation of additional experiments including ITC. Overall data analyses were performed by JC and KSR. The manuscript was written by JC, SWC and KSR.

## Peer review

The peer review history for this article is available at <https://publons.com/publon/10.1111/febs.16360>.

## Data availability statement

The data that supports the findings of this study are available in the supplementary material of this article.

## References

- Peng J, Ren KD, Yang J, Luo XJ. Mitochondrial E3 ubiquitin ligase 1: a key enzyme in regulation of

- mitochondrial dynamics and functions. *Mitochondrion*. 2016;**28**:49–53.
- Olszewska DA, Lynch T. MUL1-A new potential for a therapeutic target for Parkinson's disease a commentary on "MUL1 acts in parallel to the PINK1/parkin pathway in regulating mitofusin and compensates for loss of PINK1/parkin" by Yun and colleagues (eLife 2014; 3: 1–26). *Mov Disord*. 2016;**31**:1037.
- Yun J, Puri R, Yang H, Lizzio MA, Wu C, Sheng ZH, et al. MUL1 acts in parallel to the PINK1/parkin pathway in regulating mitofusin and compensates for loss of PINK1/parkin. *eLife*. 2014;**3**:e01958.
- Neuspiel M, Schauss AC, Braschi E, Zunino R, Rippstein P, Rachubinski RA, et al. Cargo-selected transport from the mitochondria to peroxisomes is mediated by vesicular carriers. *Curr Biol*. 2008;**18**:102–8.
- Li W, Bengtson MH, Ulbrich A, Matsuda A, Reddy VA, Orth A, et al. Genome-wide and functional annotation of human E3 ubiquitin ligases identifies MULAN, a mitochondrial E3 that regulates the organelle's dynamics and signaling. *PLoS One*. 2008;**3**:e1487.
- Zhang B, Huang J, Li HL, Liu T, Wang YY, Waterman P, et al. GIDE is a mitochondrial E3 ubiquitin ligase that induces apoptosis and slows growth. *Cell Res*. 2008;**18**:900–10.
- Jung JH, Bae S, Lee JY, Woo SR, Cha HJ, Yoon Y, et al. E3 ubiquitin ligase Hades negatively regulates the exonuclear function of p53. *Cell Death Differ*. 2011;**18**:1865–75.
- Zemirli N, Pourcelot M, Ambroise G, Hatchi E, Vazquez A, Arnoult D. Mitochondrial hyperfusion promotes NF-kappaB activation via the mitochondrial E3 ligase MULAN. *FEBS J*. 2014;**281**:3095–112.
- Bae S, Kim SY, Jung JH, Yoon Y, Cha HJ, Lee H, et al. Akt is negatively regulated by the MULAN E3 ligase. *Cell Res*. 2012;**22**:873–85.
- Rodriguez MS, Desterro JM, Lain S, Lane DP, Hay RT. Multiple C-terminal lysine residues target p53 for ubiquitin-proteasome-mediated degradation. *Mol Cell Biol*. 2000;**20**:8458–67.
- Lee SO, Lee CK, Ryu KS, Chi SW. The RING domain of mitochondrial E3 ubiquitin ligase 1 and its complex with Ube2D2: crystallization and X-ray diffraction. *Acta Crystallogr Sect F Struct Biol Cryst Commun*. 2020;**76**:1–7.
- Pickart CM. Back to the future with ubiquitin. *Cell*. 2004;**116**:181–90.
- Deshaies RJ, Joazeiro CA. RING domain E3 ubiquitin ligases. *Annu Rev Biochem*. 2009;**78**:399–434.
- Lee MS, Lee SO, Lee MK, Yi GS, Lee CK, Ryu KS, et al. Solution structure of MUL1-RING domain and its interaction with p53 transactivation domain. *Biochem Biophys Res Commun*. 2019;**516**:533–9.

- 15 Pruneda JN, Littlefield PJ, Soss SE, Nordquist KA, Chazin WJ, Brzovic PS, et al. Structure of an E3: E2~Ub complex reveals an allosteric mechanism shared among RING/U-box ligases. *Mol Cell*. 2012;**47**:933–42.
- 16 Buetow L, Gabrielsen M, Anthony NG, Dou H, Patel A, Aitkenhead H, et al. Activation of a primed RING E3-E2-ubiquitin complex by non-covalent ubiquitin. *Mol Cell*. 2015;**58**:297–310.
- 17 Stewart MD, Ritterhoff T, Klevit RE, Brzovic PS. E2 enzymes: more than just middle men. *Cell Res*. 2016;**26**:423–40.
- 18 Dou H, Buetow L, Sibbet GJ, Cameron K, Huang DT. BIRC7-E2 ubiquitin conjugate structure reveals the mechanism of ubiquitin transfer by a RING dimer. *Nat Struct Mol Biol*. 2012;**19**:876–83.
- 19 Reddy JG, Pratihari S, Ban D, Frischkorn S, Becker S, Griesinger C, et al. Simultaneous determination of fast and slow dynamics in molecules using extreme CPMG relaxation dispersion experiments. *J Biomol NMR*. 2018;**70**:1–9.
- 20 Choi YS, Lee YJ, Lee SY, Shi L, Ha JH, Cheong HK, et al. Differential ubiquitin binding by the acidic loops of Ube2g1 and Ube2r1 enzymes distinguishes their Lys-48-ubiquitylation activities. *J Biol Chem*. 2015;**290**:2251–63.
- 21 Brzovic PS, Lissounov A, Christensen DE, Hoyt DW, Klevit RE. A UbcH5/ubiquitin noncovalent complex is required for processive BRCA1-directed ubiquitination. *Mol Cell*. 2006;**21**:873–80.
- 22 Plechanovova A, Jaffray EG, Tatham MH, Naismith JH, Hay RT. Structure of a RING E3 ligase and ubiquitin-loaded E2 primed for catalysis. *Nature*. 2012;**489**:115–20.
- 23 Wu PY, Hanlon M, Eddins M, Tsui C, Rogers RS, Jensen JP, et al. A conserved catalytic residue in the ubiquitin-conjugating enzyme family. *EMBO J*. 2003;**22**:5241–50.
- 24 Pruneda JN, Stoll KE, Bolton LJ, Brzovic PS, Klevit RE. Ubiquitin in motion: structural studies of the ubiquitin-conjugating enzyme approximately ubiquitin conjugate. *Biochemistry*. 2011;**50**:1624–33.
- 25 Metzger MB, Pruneda JN, Klevit RE, Weissman AM. RING-type E3 ligases: master manipulators of E2 ubiquitin-conjugating enzymes and ubiquitination. *Biochem Biophys Acta*. 2014;**1843**:47–60.
- 26 Dove KK, Klevit RE. RING-between-RING E3 ligases: emerging themes amid the variations. *J Mol Biol*. 2017;**429**:3363–75.
- 27 Ha JH, Shin JS, Yoon MK, Lee MS, He F, Bae KH, et al. Dual-site interactions of p53 protein transactivation domain with anti-apoptotic Bcl-2 family proteins reveal a highly convergent mechanism of divergent p53 pathways. *J Biol Chem*. 2013;**288**:7387–98.
- 28 Chi SW, Lee SH, Kim DH, Ahn MJ, Kim JS, Woo JY, et al. Structural details on mdm2-p53 interaction. *J Biol Chem*. 2005;**280**:38795–802.
- 29 Bugge K, Brakti I, Fernandes CB, Dreier JE, Lundsgaard JE, Olsen JG, et al. Interactions by disorder - a matter of context. *Front Mol Biosci*. 2020;**7**:110.
- 30 Buetow L, Huang DT. Structural insights into the catalysis and regulation of E3 ubiquitin ligases. *Nat Rev Mol Cell Biol*. 2016;**17**:626–42.
- 31 Middleton AJ, Zhu J, Day CL. The RING domain of RING finger 12 efficiently builds degradative ubiquitin chains. *J Mol Biol*. 2020;**432**:3790–801.
- 32 Vaseva AV, Moll UM. The mitochondrial p53 pathway. *Biochem Biophys Acta*. 2009;**1787**:414–20.
- 33 Dai CQ, Luo TT, Luo SC, Wang JQ, Wang SM, Bai YH, et al. p53 and mitochondrial dysfunction: novel insight of neurodegenerative diseases. *J Bioenerg Biomembr*. 2016;**48**:337–47.
- 34 Chi SW. Structural insights into the transcription-independent apoptotic pathway of p53. *BMB Rep*. 2014;**47**:167–72.
- 35 Li CH, Cheng YW, Liao PL, Kang JJ. Translocation of p53 to mitochondria is regulated by its lipid binding property to anionic phospholipids and it participates in cell death control. *Neoplasia*. 2010;**12**:150–60.
- 36 Uversky VN, Oldfield CJ, Dunker AK. Intrinsically disordered proteins in human diseases: introducing the D2 concept. *Annual Review of Biophysics*. 2008;**37**:215–46.
- 37 Lee SY, Choi YS, Kim EH, Cheong HK, Lee YJ, Lee JG, et al. Nonenzymatic acetylation of ubiquitin Lys side chains is modulated by their neighboring residues. *FEBS J*. 2018;**285**:1277–89.
- 38 Gill SC, von Hippel PH. Calculation of protein extinction coefficients from amino acid sequence data. *Anal Biochem*. 1989;**182**:319–26.
- 39 Kim J, Choi D, Park C, Ryu KS. Per-deuteration and NMR experiments for the backbone assignment of 62 kDa protein, Hsp31. *J Korean Magn Reson Soc*. 2015;**19**:112–8.
- 40 Choi YS, Jeon YH, Ryu KS, Cheong C. 60th residues of ubiquitin and Nedd8 are located out of E2-binding surfaces, but are important for K48 ubiquitin-linkage. *FEBS Lett*. 2009;**583**:3323–8.
- 41 Delaglio F, Grzesiek S, Vuister GW, Zhu G, Pfeifer J, Bax A. NMRPipe: a multidimensional spectral processing system based on UNIX pipes. *J Biomol NMR*. 1995;**6**:277–93.
- 42 Lee W, Tonelli M, Markley JL. NMRFAM-SPARKY: enhanced software for biomolecular NMR spectroscopy. *Bioinformatics*. 2015;**31**:1325–7.
- 43 Otwinowski Z, Minor W. Processing of X-ray diffraction data collected in oscillation mode. *Methods Enzymol*. 1997;**276**:307–26.
- 44 McCoy AJ. Solving structures of protein complexes by molecular replacement with Phaser. *Acta Crystallogr D Biol Crystallogr*. 2007;**63**:32–41.

- 45 Kelley LA, Mezulis S, Yates CM, Wass MN, Sternberg MJ. The Phyre2 web portal for protein modeling, prediction and analysis. *Nat Protoc.* 2015;**10**:845–58.
- 46 Emsley P, Lohkamp B, Scott WG, Cowtan K. Features and development of Coot. *Acta Crystallogr D Biol Crystallogr.* 2010;**66**:486–501.
- 47 Adams PD, Afonine PV, Bunkoczi G, Chen VB, Davis IW, Echols N, et al. PHENIX: a comprehensive Python-based system for macromolecular structure solution. *Acta Crystallogr D Biol Crystallogr.* 2010;**66**:213–21.
- 48 Williams CJ, Headd JJ, Moriarty NW, Prisant MG, Videau LL, Deis LN, et al. MolProbity: more and better reference data for improved all-atom structure validation. *Protein Sci.* 2018;**27**:293–315.
- 49 Pettersen EF, Goddard TD, Huang CC, Couch GS, Greenblatt DM, Meng EC, et al. UCSF Chimera—a visualization system for exploratory research and analysis. *J Comput Chem.* 2004;**25**:1605–12.
- 50 Schwieters CD, Bermejo GA, Clore GM. Xplor-  
NIH for molecular structure determination from NMR and other data sources. *Protein Sci.* 2018;**27**:26–40.

### Supporting information

Additional supporting information may be found online in the Supporting Information section at the end of the article.

**Fig. S1.** The interactions between RING<sub>MULTI</sub> and UBE2D2 were monitored by <sup>1</sup>H–<sup>15</sup>N HSQC experiments.

**Fig. S2.** The representative ITC data of the RING<sub>MULTI</sub>-mediated interactions.

**Table S1.** Statistics of data collections and structure refinements.